NAVAL POSTGRADUATE SCHOOL
Monterey, California

THESIS

SIMULATIONS OF LANL REGENERATIVE MW FREE ELECTRON LASER AMPLIFIER

by

Richard T. Nguyen

December 1997

Thesis Advisor: William B. Colson
                                    Robert L. Armstead

Approved for public release; distribution is unlimited.

REPORT DOCUMENTATION PAGE

Public reporting burden for this collection of information is estimated to average 1 hour per response, including the time for reviewing instruction, searching existing data sources, gathering and maintaining the data needed, and completing and reviewing the collection of information. Send comments regarding this burden estimate or any other aspect of this collection of information, including suggestions for reducing this burden, to Washington headquarters Services, Directorate for Information Operations and Reports, 1215 Jefferson Davis Highway, Suite 1204, Arlington, VA 22202-4302, and to the Office of Management and Budget, Paperwork Reduction Project (0704-0188) Washington DC 20503.

1. AGENCY USE ONLY *(Leave blank)*	2. REPORT DATE December 1997	3. REPORT TYPE AND DATES COVERED Master's Thesis

4. TITLE AND SUBTITLE SIMULATIONS OF LANL REGENERATIVE MW FREE ELECTRON LASER AMPLIFIER	5. FUNDING NUMBERS
6. AUTHOR(S) Richard T. Nguyen	

7. PERFORMING ORGANIZATION NAME(S) AND ADDRESS(ES) Naval Postgraduate School Monterey, CA 93943-5000	8. PERFORMING ORGANIZATION REPORT NUMBER

9. SPONSORING / MONITORING AGENCY NAME(S) AND ADDRESS(ES)	10. SPONSORING/ MONITORING AGENCY REPORT NUMBER

11. SUPPLEMENTARY NOTES

The views expressed in this thesis are those of the author and do not reflect the official policy or position of the Department of Defense or the U.S. Government.

12a. DISTRIBUTION / AVAILABILITY STATEMENT Approved for public release; distribution is unlimited.	12b. DISTRIBUTION CODE

13. ABSTRACT *(maximum 200 words)*

The development of a speed-of-light hard-kill weapon system for military applications represents a significant advancement in technology over present conventional kinetic weapon systems. Over the past two decades, the US Navy has successfully developed a megawatt-class chemical laser; however, under some maritime environments, the high power beam propagation was unable to delivery sufficient energy to kill a modern anti-ship missile (ASM) due to significant atmospheric absorption and the resulting thermal blooming process. A critical problem to resolve for the shipboard high-energy laser weapon systems is to develop a shipboard-compatible megawatt-class laser weapon at a wavelength where the atmospheric absorption is smallest. The megawatt-class Free Electron Laser (FEL) has significant advantages over conventional weapon systems and other chemical high-energy laser systems. Infinite magazine, rapid response, and wavelength tunability make the FEL a suitable and desirable shipboard weapon system.

This thesis divides into four chapters. Chapters I and II introduce the FEL and background theory of the FEL. Chapter III explores the analysis of the LANL Regenerative MW FEL Amplifier design and optimizes its efficiency. Lastly, chapter IV summarizes the feasibility of achieving the desired efficiency.

14. SUBJECT TERMS Simulations of LANL Regenerative MW Free Electron Laser Amplifier	15. NUMBER OF PAGES 60
	16. PRICE CODE

17. SECURITY CLASSIFICATION OF REPORT Unclassified	18. SECURITY CLASSIFICATION OF THIS PAGE Unclassified	19. SECURITY CLASSIFICATION OF ABSTRACT Unclassified	20. LIMITATION OF ABSTRACT UL

SIMULATIONS OF LANL REGENERATIVE MW
FREE ELECTRON LASER AMPLIFIER

Richard T. Nguyen

Lieutenant, United States Navy

B. A., University of California San Diego, 1986

Submitted in partial fulfillment of the

requirements for the degree of

MASTER OF SCIENCE IN APPLIED PHYSICS

from the

NAVAL POSTGRADUATE SCHOOL

December 1997

ABSTRACT

The development of a speed-of-light hard-kill weapon system for military applications represents a significant advancement in technology over present conventional kinetic weapon systems. Over the past two decades, the US Navy has successfully developed a megawatt-class chemical laser; however, under some maritime environments, the high power beam propagation was unable to delivery sufficient energy to kill a modern anti-ship missile (ASM) due to significant atmospheric absorption and the resulting thermal blooming process. A critical problem to resolve for the shipboard high-energy laser weapon systems is to develop a shipboard-compatible megawatt-class laser weapon at a wavelength where the atmospheric absorption is smallest. The megawatt-class Free Electron Laser (FEL) has significant advantages over conventional weapon systems and other chemical high-energy laser systems. Infinite magazine, rapid response, and wavelength tunability make the FEL a suitable and desirable shipboard weapon system.

This thesis divides into four chapters. Chapters I and II introduce the FEL and background theory of the FEL. Chapter III explores the analysis of the LANL Regenerative MW FEL Amplifier design and optimizes its efficiency. Lastly, chapter IV summarizes the feasibility of achieving the desired efficiency.

TABLE OF CONTENTS

ACKNOWLEDGEMENT

The author gratefully acknowledges the guidance, advice, and attention to detail of Professors W. B. Colson and R. L. Armstead. The author would also like to thank to Dr. R. K. Wong for his efforts in assisting computer simulations. Their patience, insight, and technical assistance were invaluable.

Finally, this thesis would not have been possible without the love and support of my wonderful wife KimChi, and my beautiful daughter Alisa. Thank you!

I. INTRODUCTION

A.   DEFENSE AT THE SPEED OF LIGHT

In today's technology, weapon systems rely predominantly on kinetic kill, striking a missile with another missile or with several bullets. These weapons are relatively slow and require a longer detect-to-engage sequence when factoring in tracking time, launch time and time of flight to intercept. In searching for faster and faster weapons and ever-decreasing response times, Directed Energy Weapons (DEW) have been on the U.S. military's "love to have" list for several decades. DEWs are attractive for several reasons, and the most predominant reason is that they offer speed-of-light defense.

In 1971, the U.S. Navy established the Navy High Energy Laser (HEL) Program with the intentions of developing speed-of-light hard-kill weapon system. Initial development focused on building a CO_2 gas dynamic laser technology, but a few years later its emphasis shifted to continuous-wave deuterium fluoride (DF) chemical lasers because they propagate far better in the maritime environments. In the early 1980s, the megawatt class Mid-Infrared Advanced Chemical Laser (MIRACL) was built by TRW for the Navy as the highest average power continuous wave (CW) laser in the west. The SeaLite Beam Director (SLBD) was built by Hughes Aircraft to accommodate and direct the MIRACL beam. The MIRACL and SLBD have successfully tested at White Sands Missile Range, New Mexico, in engaging and destroying several types of missiles in flight [1].

Although the MIRACLE/SLBD system was successfully tested against crossing targets in a fleet defense scenario, its lethality was not sufficient in some ship self-defense engagement scenarios due to insufficient crosswind [1]. Insufficient crosswind will cause the laser beam heating the air in its own path resulting in a defocusing optical lens known as thermal blooming [2]. The thermal blooming effect can severely reduce the High Energy Laser Weapon Systems' (HELWS) lethal range. As a result, it's necessary to replace the MIRACL with a megawatt-class laser device at a wavelength where

1

atmospheric absorption is smallest. An ideal solution is the megawatt-class Free Electron Laser (FEL) that is tunable to the optimum propagation wavelength.

B.   SHORT HISTORY OF FREE ELECTRON LASER

The first generation of coherent radiation from free electron beams was microwave tubes that relied on slow-wave structures, and their development received a significant impact from the radar development during World War II. In 1951, Motz showed that an electron beam propagating through an undulator magnet can be used to amplify radiation. After 1960, research on short wavelength lasers has been dominant, but they require an atomic or molecular medium to operate, resulting in a limitation on wavelength tunability. In 1971, J. M. J. Madey of Stanford University brought attention to what he proposed as the 'free electron laser'. Relying on research of synchrotron radiation sources, Madey conceived a device that would lase in the visible using a beam of relativistic electrons as the source. In 1976, the first successful free electron laser (FEL) experiment was demonstrated by Madey and his co-workers at Stanford University, in that they measured 7% gain from an FEL configured as an amplifier at $10\,\mu m$ wavelength. One year later, another successful FEL operation of the same FEL configured as an oscillator. These successful experiments created a large interest in FEL research. Since then, scientist and experimental groups around the world built FELs that operate at frequencies ranging from microwave to the UV [11]. Three other FELs were built soon after. The first was built at Laboratoire pour l'Utilisation du Rayonment Electromagnetique in Orsay, France, which operated in the visible range. The second involved a team from TRW at Stanford using the Superconducting Accelerator (SCA), lasing in the near infrared (IR). The third was built at Los Alamos that lased in the mid-infrared [3]. Now, there are many FELs used for research around the world.

C. BASIC FREE ELECTRON LASER THEORY

The FEL is a device that transforms the kinetic energy of a relativistic electron beam into electromagnetic (EM) radiation [4]. This is accomplished by sending a relativistic electron beam from a linear accelerator, microtron or a storage ring etc., through an alternating magnetic field produced by a device known as an undulator as shown in Figure 1.1. The interaction of the negatively charged electrons with the spatially periodic magnetic field induces a transverse acceleration on the electrons that causes them to exchange energy with a copropagating radiation field. The kinetic energy extracted from the electron beam is converted to electromagnetic radiation. The energy of the electron beam and the period of the undulator magnet determine the wavelength of radiation. This system provides a powerful source of tunable, coherent, electromagnetic radiation that can operate in a wavelength range from about 1 cm to the X-ray region. This system can also provide continuous wave (CW) operation, or very short pulses in the nanosecond, picosecond, or even subpicosecond region.

Electron Beam

Undulator

Resonator   **Mirror**
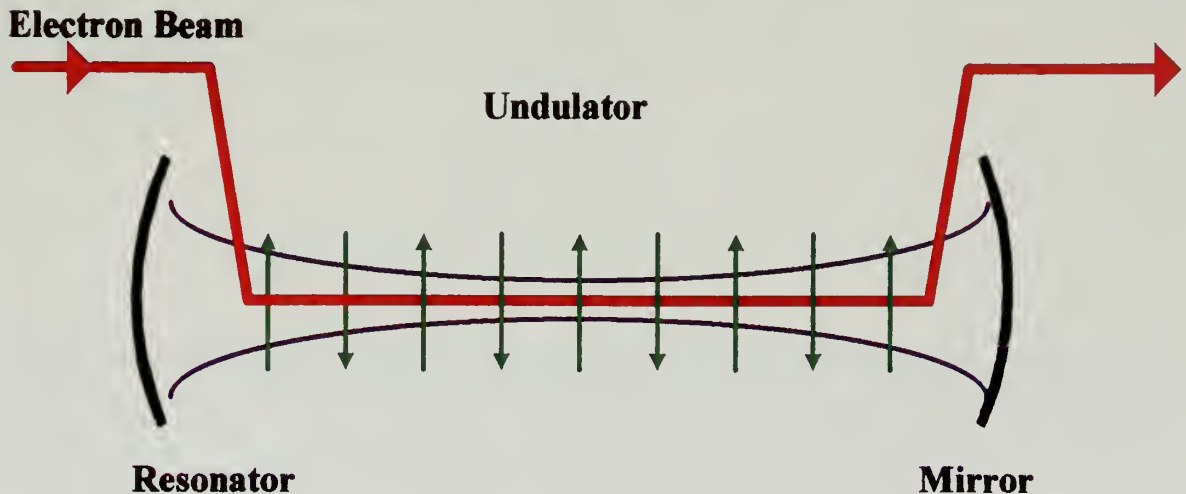
Figure 1.1. Schematic diagram of a free electron laser.

II. PRINCIPLES OF OPERATION OF FEL

A.   ELECTRON TRAJECTORY IN THE UNDULATOR

For better understanding of the physical mechanism underlying the operation of an FEL, we first consider the interaction of a free electron in the undulator and an electromagnetic wave. The Lorentz force equation and the equation for the energy exchange between the electron and the electromagnetic wave are

$$\bar{F} = \frac{d\bar{p}}{dt} = -e\left(\bar{E} + \frac{\bar{v}}{c} \times \bar{B}\right), \tag{2.1}$$

$$\frac{d(\gamma mc^2)}{dt} = -e\,\bar{v} \cdot \bar{E}, \tag{2.2}$$

where e, m and $\bar{v}$ are the charge, mass and velocity of the electron, respectively; γ is the relativistic factor of the electron, $\gamma = 1/\sqrt{(1-\bar{\beta}^2)}$; $\bar{\beta} = \bar{v}/c$; $\bar{p}$ is the relativistic momentum of the electron, $\bar{p} = \gamma m\bar{v}$; $\bar{E}$ is the electric field of the EM wave; $\bar{B}$ is the magnetic field ; γmc^2 is the electron energy; and c is the speed of light in vacuum [5].

Considering an electron with velocity $\bar{v} = \bar{\beta}\,c$ and a transverse electromagnetic wave propagating colinearly, in the z-direction in a vacuum, then equations (2.1) and (2.2) become

$$\frac{d(\gamma\,\bar{\beta})}{dt} = -\frac{e}{mc}\left(\bar{E} + \bar{\beta} \times \bar{B}\right), \tag{2.3}$$

$$\frac{d\gamma}{dt} = -\frac{e}{mc}\,\bar{\beta} \cdot \bar{E}. \tag{2.4}$$

Assume the undulator has a helical magnetic field of the form $\bar{B} = B[\cos(k_o z), \sin(k_o z), 0]$, where $k_o = 2\pi / \lambda_o$ is the undulator wavenumber, and λ_o is the undulator wavelength. The corresponding circular-polarized, plane-wave optical field is then

$$\bar{E}_s = E(\cos\psi, -\sin\psi, 0), \text{ and } \bar{B}_s = E(\sin\psi, \cos\psi, 0),$$

where $\psi = kz - \omega t + \phi$. E is the electric and magnetic field amplitude in cgs units, t is time, ϕ is the optical phase, $k = \omega / c$ is the optical wavenumber, and ω is the optical angular frequency. Substituting the fields into Lorentz force equations yields

5

$$\frac{d(\gamma\bar{\beta}_\perp)}{dt} = -\frac{e}{mc}[E(1-\beta_z)(\cos\psi,-\sin\psi,0) + \beta_z B(-\sin(k_o z),\cos(k_o z),0)], \quad (2.5)$$

$$\frac{d(\gamma\beta_z)}{dt} = -\frac{e}{mc}[E(\beta_x\cos\psi - \beta_y\sin\psi) + B(\beta_x\sin(k_o z) - \beta_y\cos(k_o z))], \quad (2.6)$$

$$\text{and} \quad \frac{d\gamma}{dt} = -\frac{e}{mc}E(\beta_x\cos\psi - \beta_y\sin\psi), \quad (2.7)$$

where $\bar{\beta} = \bar{\beta}_\perp + \bar{\beta}_z$, $\bar{\beta}_\perp = \beta_x\hat{i} + \beta_y\hat{j}$, and $\bar{\beta}_z = \beta_z\hat{k}$. For relativistic electrons, $\beta_z \approx 1$, hence $E(1-\beta_z) \ll \beta_z B$, so in the right-hand side of (2.5) the first term is ignored. The second term is

$$\frac{d(\gamma\bar{\beta}_\perp)}{dt} = -\frac{eB\beta_z}{mc}(-\sin(k_o z),\cos(k_o z),0). \quad (2.8)$$

Integrating the transverse equation (2.8) and assuming a perfect injection of electron beam into the undulator cavity, which makes the constant of integration zero, yields

$$\gamma\bar{\beta}_\perp = -\left(\frac{eB}{mc^2}\right)(\cos(k_o z),\sin(k_o z),0). \quad (2.9)$$

Divide both side of (2.9) by γ to get

$$\bar{\beta}_\perp(z) = -\frac{K}{\gamma}(\cos(k_o z),\sin(k_o z),0), \quad (2.10)$$

where the undulator parameter is $K = eB/k_o mc^2 = eB\lambda_o/2\pi mc^2$. Equation (2.10) describes the transverse motion of electrons in the helical undulator [6].

B.   FEL RESONANCE -- ELECTRON AND PHOTON RACE

Accelerated electrons traveling at a relativistic speed along the longitudinal axis of the undulator of the FEL radiate optical energy [6]. In order for the FEL to have gain (i.e. the fractional change in optical power in a single pass through the undulator), a net transfer of energy from the electron beam to the optical beam must occur. In order for an optimum exchange of energy from an electron to the optical field to occur, the electron must oscillate in phase with the optical field. This optimum energy exchange occurs when the electron falls behind the optical fields by a distance of one optical wavelength within the span of one undulator period [6].

6

Speed of electron $\beta_z c$

Speed of light c

λ

Light wavelength

t=0　　　　　　Undulator wavelength λ_o　　　　t=$\lambda_o/\beta_z c$
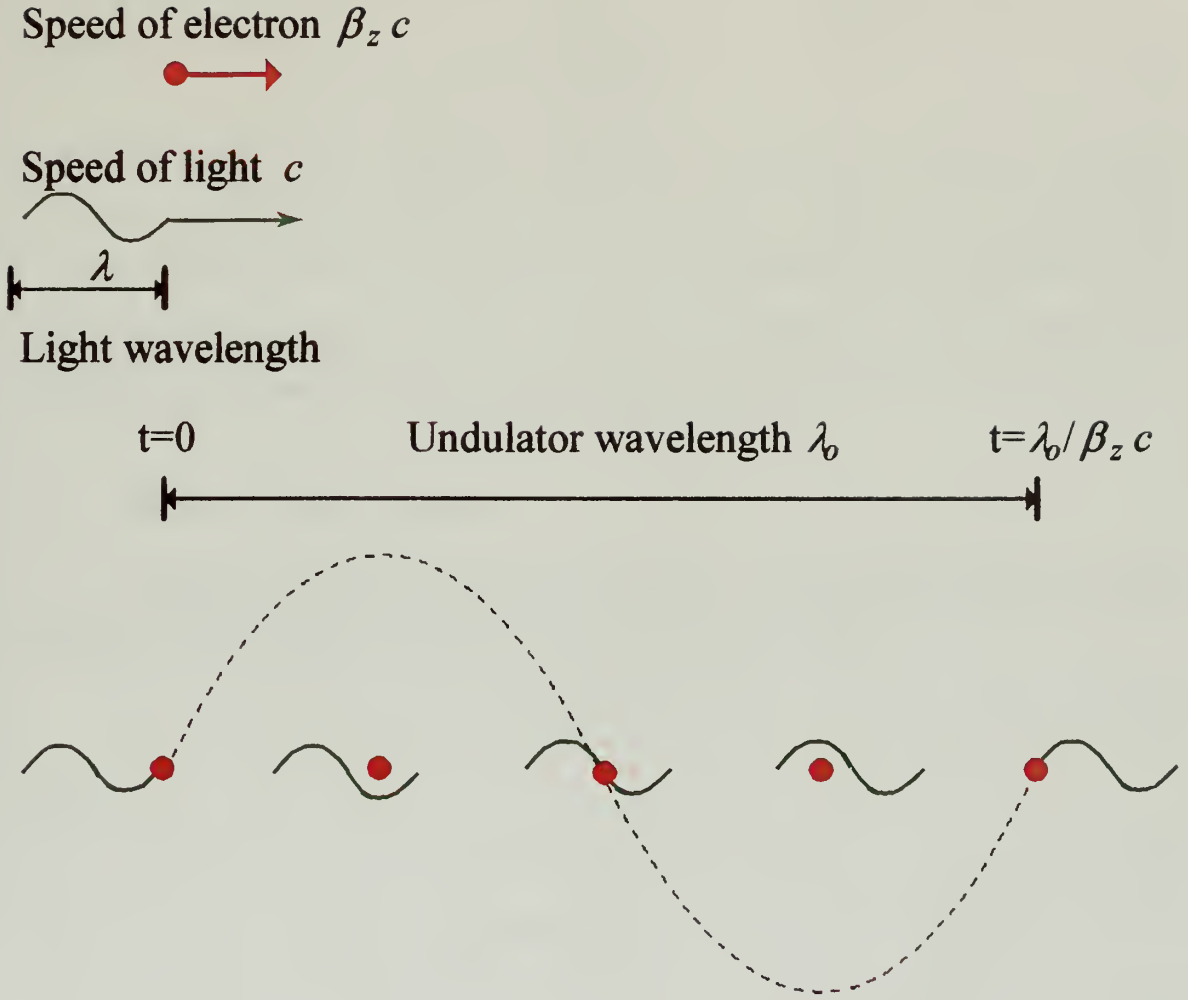
Figure 2.1. Electron-Photon race.

Consider an optical wave that travels at speed c and passes over an electron traveling at speed $\beta_z c$ as shown in Figure 2.1. At resonance condition, one wavelength of the optical wave passes over an electron while it travels through one undulator wavelength λ_o, so that light wavelength $\lambda = (c - \beta_z c)t$. Insert $t = \lambda_o / \beta_z c$ yielding $\lambda = \dfrac{1 - \beta_z}{\beta_z} \lambda_o$. Substitute

$\beta_\perp^2 = \dfrac{K^2}{\gamma^2}$ into $\gamma^{-2} = 1 - \beta^2 = 1 - \beta_z^2 - \beta_\perp^2$ yields

$$(1 + K^2)\gamma^{-2} = 1 - \beta_z^2 . \qquad (2.11)$$

7

Since $\beta_z \approx 1$, $1 - \beta_z \approx \dfrac{1 + K^2}{2\gamma^2}$, then

$$\lambda = \lambda_o \frac{1 + K^2}{2\gamma^2} \, .\tag{2.12}$$

The equation (2.12) is the resonance condition that demonstrates the tunability of the FEL. By adjusting the undulator parameter K, or the energy of the electron beam $(\gamma - 1)mc^2$ or the undulator wavelength λ_o, the wavelength of the optical field can be tuned to a desired wavelength within a prescribed bandwidth [7]. This is a significant advantage over conventional lasers that are typically constrained to a fixed wavelength.

C. PENDULUM EQUATION

This section derives the equation of motion of the electrons resulting from the interaction with the optical field. Substitute (2.10) into (2.7) to get

$$\dot{\gamma} = \frac{eKE}{\gamma mc} \cos(\zeta + \phi),\tag{2.13}$$

where

$$\zeta + \phi = \psi + k_o z = (k + k_o)z - \omega t + \phi \, .\tag{2.14}$$

For $-\pi/2 < \zeta + \phi < \pi/2$, the cosine function in (2.13) is positive and the electrons will gain energy from the optical field, whereas for $\pi/2 < \zeta + \phi < 3\pi/2$, the cosine is negative and the electrons will lose energy to the optical field. Differentiating (2.11) with respect to time t gives $2\gamma^{-3}\dot{\gamma}(1 + K^2) = 2\beta_z \dot{\beta}_z$. Relating $\dot{\gamma}$ to $\dot{\beta}_z$ gives

$$\frac{\dot{\gamma}}{\gamma} = \frac{\gamma^2 \beta_z \dot{\beta}_z}{(1 + K^2)} \, .\tag{2.15}$$

Differentiating (2.14) once yields $\dot{\zeta} = (k + k_o)\dot{z} - \omega = (k + k_o)c\beta_z - \omega$, and differentiating twice yields $\ddot{\zeta} = (k + k_o)c\dot{\beta}_z$. Insert the resulting expression for $\dot{\beta}_z$ into (2.15) to get

$$\frac{\dot{\gamma}}{\gamma} = \frac{\gamma^2 \beta_z \ddot{\zeta}}{(1 + K^2)(k + k_o)c} \, .\tag{2.16}$$

8

Since $\lambda \ll \lambda_o$, then $k_o \ll k$, so $(k + k_o)c \approx kc = \omega$. Using this approximation and the resonance condition (2.12), equation (2.16) becomes

$$\frac{\dot{\gamma}}{\gamma} \approx \frac{\gamma^2 \ddot{\zeta}}{(1+K^2)\omega} = \frac{\ddot{\zeta}}{2\omega_o}. \tag{2.17}$$

So, $\dfrac{\ddot{\zeta}}{2\omega_o} = \dfrac{\dot{\gamma}}{\gamma} = \dfrac{eKE}{\gamma^2 mc}\cos(\zeta + \phi)$, then the electron equation of motion is

$$\ddot{\zeta} = \frac{2\omega_o eKE}{\gamma^2 mc}\cos(\zeta + \phi). \tag{2.18}$$

Equation (2.18) describes the electron phase dynamics in the form of the pendulum equation [6].

Consider time evolution through the undulator $L/\beta_o c$ for an average electron, where L is the length of the undulator. Introducing relevant dimensionless time $\tau = \beta_0 ct/L \approx ct/L$, we see that τ will vary between 0 and 1 along the undulator length. Substituting $dt = (L/c)d\tau$ into the pendulum equation (2.18) gives

$$\overset{\circ\circ}{\zeta} = \overset{\circ}{v} = |a|\cos(\zeta + \phi), \tag{2.19}$$

where the notation $(\overset{\circ}{..}) \equiv d(..)/d\tau$, $|a| = 4\pi NeKLE/\gamma^2 mc^2$ is the dimensionless optical field strength, and $N = L/\lambda_o$ is the total number of undulator periods. Equation (2.19) is the electron pendulum equation that governs the phase-space motion of the electrons within the undulator and under the influence of the optical wave [6].

D.   OPTICAL WAVE EQUATION

An electromagnetic wave will propagate in the absence of a current density according to

$$\left(\nabla^2 - \frac{1}{c^2}\frac{\partial^2}{\partial t^2}\right)\bar{A}(\bar{r},t) = 0, \qquad (2.20)$$

where the Laplacian is $\nabla^2 = \partial_x^2 + \partial_y^2 + \partial_z^2$, $\bar{r}$ is the vector position, t is time, and $\bar{A}$ is the optical vector potential [5]. The optical electric and magnetic fields can be expressed in terms of the vector potential by the following relationships

$$\bar{E} = -\frac{1}{c}\frac{\partial \bar{A}}{\partial t}, \qquad (2.21)$$

and

$$\bar{B} = \bar{\nabla}\times\bar{A}. \qquad (2.22)$$

Assuming that the optical beam is a circularly polarized plane wave, then the vector potential has the form

$$\bar{A} = \frac{E(\bar{r},t)}{k}(\sin\psi,\cos\psi,0) = \Re e\left\{\frac{1}{k}\mathscr{E}(\bar{r},t)\hat{e}e^{i(kz-\omega t)}\right\}, \qquad (2.23)$$

where $\mathscr{E}(\bar{r},t) = E(\bar{r},t)e^{i\phi(\bar{r},t)}$, $\psi = kz - \omega t + \phi$ is the plane-wave phase, $\hat{e} = (-i,1,0)$ is the polarization vector, $k = 2\pi c/\omega$ is the optical wave number, ω is the optical frequency, and $\phi(\bar{r},t)$ is the optical phase [7]. For convenience, we write

$$\bar{A} = \frac{1}{k}\mathscr{E}(\bar{r},t)\hat{e}e^{i\alpha}, \qquad (2.24)$$

where $\alpha = kz - \omega t$. Differentiating (2.24) with respect to t gives

$$\frac{\partial \bar{A}}{\partial t} = \frac{\hat{e}}{k}\left(\dot{\mathscr{E}} - i\omega\mathscr{E}\right)e^{i\alpha}, \qquad (2.25)$$

where $\dot{(..)}\equiv\partial(..)/\partial t$. Differentiating (2.25) with respect to t gives

$$\frac{\partial^2 \bar{A}}{\partial t^2} = \frac{\hat{e}}{k}\left(\ddot{\mathscr{E}} - 2i\omega\dot{\mathscr{E}} - \omega^2\mathscr{E}\right)e^{i\alpha}, \qquad (2.26)$$

where $\ddot{(..)}\equiv\partial^2(..)/\partial t^2$. Differentiate (2.24) with respect to z gives

10

$$\frac{\partial \bar{A}}{\partial z} = \frac{\hat{e}}{k}\left(\mathcal{E}' - ik\,\mathcal{E}\right)e^{i\alpha} , \tag{2.27}$$

where $(..)' \equiv \partial(..)/\partial z$. Differentiate (2.27) with respect to z gives

$$\frac{\partial^2 \bar{A}}{\partial z^2} = \frac{\hat{e}}{k}\left(\mathcal{E}'' + 2ik\,\mathcal{E}' - k^2\mathcal{E}\right)e^{i\alpha} , \tag{2.28}$$

where $(..)'' \equiv \partial^2(..)/\partial z^2$. Since the laser beam consists of a narrow range of frequencies, the variation in the electric field amplitude and phase with respect to space over an optical wavelength λ is small, so that $\mathcal{E}' \ll k\mathcal{E}$ and $\phi' \ll k\phi$. The variation in the electric field amplitude and phase with respect to time over an optical period is also small, so that $\dot{\mathcal{E}} \ll \omega\,\mathcal{E}$ and $\dot{\phi} \ll \omega\phi$ [7]. Therefore, $\mathcal{E}''$ is negligible compare to $k\mathcal{E}'$, and $\ddot{\mathcal{E}}$ is negligible compare to $\omega\dot{\mathcal{E}}$, then (2.26) can be simplified to

$$\frac{\partial^2 \bar{A}}{\partial t^2} = \frac{\hat{e}e^{i\alpha}}{k}\left(-2i\omega\dot{\mathcal{E}} - \omega^2\mathcal{E}\right), \tag{2.29}$$

and (2.28) can be simplified as

$$\frac{\partial^2 \bar{A}}{\partial z^2} = \frac{\hat{e}e^{i\alpha}}{k}\left(2ik\,\mathcal{E}' - k^2\mathcal{E}\right). \tag{2.30}$$

Substitute (2.29) and (2.30) into the left hand side of (2.20) yields

$$\left(\nabla^2 - \frac{1}{c^2}\frac{\partial^2}{\partial t^2}\right)\bar{A}(\bar{r},t) = \frac{\hat{e}e^{i\alpha}}{k}\left[\nabla_\perp^2\mathcal{E} + 2ik\left(\mathcal{E}' + \frac{1}{c}\dot{\mathcal{E}}\right)\right], \tag{2.31}$$

where $\nabla_\perp^2 = \frac{\partial^2}{\partial x^2} + \frac{\partial^2}{\partial y^2}$. Hence,

$$\left[\nabla_\perp^2 + 2ik\left(\frac{\partial}{\partial z} + \frac{1}{c}\frac{\partial}{\partial t}\right)\right]\mathcal{E} = 0. \tag{2.32}$$

The first partial second derivatives with respect to x and y describe how the beam changes due to diffraction as it propagates. The last partial derivatives with respect to z and t describe the propagation of a plane wave along the z axis.

Introduce dimensionless time $\tau = ct/L$ so that τ varies from 0 to 1 along the undulator length. It's convenient to follow the wavefront with a new coordinate $\tilde{z} = z - ct$. With this coordinate change,

11

$$\frac{\partial}{\partial z} = \left(\frac{\partial \tilde{z}}{\partial z}\right)\frac{\partial}{\partial \tilde{z}} + \left(\frac{\partial \tau}{\partial z}\right)\frac{\partial}{\partial \tau} = \frac{\partial}{\partial \tilde{z}}, \tag{2.33}$$

since $\partial \tilde{z}/\partial z = 1$ and $\partial \tau/\partial z = 0$. Also,

$$\frac{1}{c}\frac{\partial}{\partial t} = \frac{1}{c}\left[\left(\frac{\partial \tilde{z}}{\partial t}\right)\frac{\partial}{\partial \tilde{z}} + \left(\frac{\partial \tau}{\partial t}\right)\frac{\partial}{\partial \tau}\right] = -\frac{\partial}{\partial \tilde{z}} + \frac{1}{L}\frac{\partial}{\partial \tau}, \tag{2.34}$$

since $\partial \tilde{z}/\partial t = -c$ and $\partial \tau/\partial t = c/L$. Therefore, the propagation operator in (2.32) becomes

$$\frac{\partial}{\partial z} + \frac{1}{c}\frac{\partial}{\partial t} = \frac{\partial}{\partial \tilde{z}} + \left(-\frac{\partial}{\partial \tilde{z}} + \frac{1}{L}\frac{\partial}{\partial \tau}\right) = \frac{1}{L}\frac{\partial}{\partial \tau}. \tag{2.35}$$

Hence, the full wave operator is

$$\left[\nabla_\perp^2 + 2ik\left(\frac{\partial}{\partial z} + \frac{1}{c}\frac{\partial}{\partial t}\right)\right] = \left[\nabla_\perp^2 + 2ik\frac{1}{L}\frac{\partial}{\partial \tau}\right]. \tag{2.36}$$

Introducing the dimensionless transverse variables $\tilde{x} = x\sqrt{k/2L}$ and $\tilde{y} = y\sqrt{k/2L}$, so

that $\dfrac{\partial^2}{\partial x^2} = (k/2L)\dfrac{\partial^2}{\partial \tilde{x}^2}$ and $\dfrac{\partial^2}{\partial y^2} = (k/2L)\dfrac{\partial^2}{\partial \tilde{y}^2}$. Hence $\nabla_\perp^2 = (k/2L)\left(\dfrac{\partial^2}{\partial \tilde{x}^2} + \dfrac{\partial^2}{\partial \tilde{y}^2}\right) =$

$(k/2L)\tilde{\nabla}_\perp^2$, where $\tilde{\nabla}_\perp^2 = \dfrac{\partial^2}{\partial \tilde{x}^2} + \dfrac{\partial^2}{\partial \tilde{y}^2}$. Substituting into (2.36) and (2.32) yields

$$\left[\frac{-i}{4}\tilde{\nabla}_\perp^2 + \frac{\partial}{\partial \tau}\right]\mathscr{E} = 0. \tag{2.37}$$

Equation (2.36) is known as the parabolic wave equation [7]. In dimensionless parameters, the optical field is represented by $a = |a|e^{i\phi}$ where $|a| = 4\pi NeKLE/(\gamma^2 mc^2) \propto E$, so $\mathscr{E}$ and a differ by a multiplicative constant. Therefore, exchange $\mathscr{E}$ for a, the dimensionless parabolic wave equation (2.37) becomes

$$\left[\frac{-i}{4}\tilde{\nabla}_\perp^2 + \frac{\partial}{\partial \tau}\right]a = 0. \tag{2.38}$$

In the presence of the electron beam current density, the optical wave equation (2.20) is

12

$$\left(\nabla^2 - \frac{1}{c^2}\frac{\partial^2}{\partial t^2}\right)\vec{A}(\vec{r},t) = -\frac{4\pi}{c}\vec{J}_\perp, \tag{2.39}$$

where $\vec{J}_\perp$ is the transverse electron beam current density [8]. Substituting (2.30) into (2.39) yields

$$\frac{\hat{e}e^{i\alpha}}{k}\left[\nabla_\perp^2 + 2ik\left(\frac{\partial}{\partial z} + \frac{1}{c}\frac{\partial}{\partial t}\right)\right]\mathcal{E} = -\frac{4\pi}{c}\vec{J}_\perp. \tag{2.40}$$

Performing a dot product with $\hat{e}^* = (i,1,0)$ on both sides of (2.40) and using $\hat{e}^* \cdot \hat{e} = (i,1,0)\cdot(-i,1,0) = 2$, yields

$$\left[\frac{1}{2}\nabla_\perp^2 + ik\left(\frac{\partial}{\partial z} + \frac{1}{c}\frac{\partial}{\partial t}\right)\right]\mathcal{E} = -\frac{\pi k}{c}\vec{J}_\perp \cdot \hat{e}^* e^{-i\alpha}. \tag{2.41}$$

The total transverse electron beam current is the sum of all single particle currents. The single particle current for one electron in the beam is $\vec{J}_{\perp i} = -ec\vec{\beta}_\perp \delta^{(3)}(\vec{x} - \vec{r}_i)$ [8] where $\vec{r}_i$ is the position of the ith electron and $\delta^{(3)}(\vec{x}_i - \vec{r}_i)$ is the three-dimensional Dirac delta-function. The total beam current is

$$\vec{J}_\perp = \sum_i \vec{J}_{\perp i} = -ec\sum_i \vec{\beta}_\perp \delta^{(3)}(\vec{x} - \vec{r}_i). \tag{2.42}$$

From (2.10), the transverse motion is $\vec{\beta}_\perp = (-K/\gamma)(\cos k_o z, \sin k_o z, 0) =$ $\Re e\left\{(-K/\gamma)i\hat{e}e^{-ik_o z}\right\}$. For convenience, we write $\vec{\beta}_\perp = \frac{-K}{\gamma}i\hat{e}e^{-ik_o z}$, so that

$$\vec{J}_\perp \cdot \hat{e}^* e^{-i\alpha} = iecK(\hat{e}^* \cdot \hat{e})\sum_i \frac{e^{-i(k_o z + \alpha)}}{\gamma}\delta^{(3)}(\vec{x} - \vec{r}_i). \tag{2.43}$$

We can simplify the sum $\sum_i$ by assuming a local electron density ρ, so that (2.41) becomes

$$\left[\frac{1}{2}\nabla_\perp^2 + ik\left(\frac{\partial}{\partial z} + \frac{1}{c}\frac{\partial}{\partial t}\right)\right]\mathcal{E} = -2\pi iekK\rho\left\langle\frac{e^{-i\zeta}}{\gamma}\right\rangle, \tag{2.44}$$

13

where $\zeta = k_o z + \alpha$ is the electron phase in the combined undulator and optical fields, and $\langle ... \rangle$ is a weighted average of sampled electrons at a specific site which replaces the summation over all electrons within one optical wavelength. Define the dimensionless beam current $j = 8N(e\pi KL)^2 \rho/(\gamma^3 mc^2)$, the wave equation becomes

$$\left[\frac{-i}{4}\widetilde{\nabla}_\perp^2 + \frac{\partial}{\partial\tau} \right] a(x, y, \widetilde{z}, \tau) = -j\langle e^{-i\zeta} \rangle.$$ (2.45)

In some cases where the optical wave diffraction is not significant, we can ignore $\widetilde{\nabla}_\perp^2$ in (2.45), then

$$\overset{\circ}{a} = -j\langle e^{-i\zeta} \rangle.$$ (2.46)

The optical wave equation (2.46) couples the electrons to the copropagating optical wave by relating the electron phase to the change in the optical field. The equation (2.46) can be expressed in terms of amplitude and phase,

$$\overset{\circ}{|a|} = -j\langle \cos(\zeta + \phi) \rangle,$$ (2.47)

and $$\overset{\circ}{\phi} = \frac{j}{|a|}\langle \sin(\zeta + \phi) \rangle.$$ (2.48)

Equation (2.47) reveals that when the electrons become bunched near $(\zeta + \phi) \approx \pi$, the optical field amplitude will grow, and when bunched near $(\zeta + \phi) \approx 0$, the optical field amplitude will decrease. Equation (2.48) describes the optical phase evolution.

14

E. GAIN DEGRADATION DUE TO ELECTRON BEAM QUALITY

In the design of an FEL, there is often a trade-off between high beam current and good beam quality as determined by the accelerator. The dimensionless current $j \propto IN^3\lambda^{1/2}$ where I is the actual beam current, N is the number of undulator periods, and λ is the optical wavelength. Usually the optical wavelength λ is fixed for a given application so that j is maximized by adjusting current I and the undulator periods N. Increasing I tends to degrade the beam quality from the accelerator, whereas increasing N tends to increase the FEL sensitivity to the beam quality because of narrowing the gain spectrum bandwidth [9].

Emittance ε describes one aspect of electron beam quality. A real electron beam has an emittance ε describing how electrons enter the undulator with a range of angles θ_x with respect to the undulator axis, and at a range of transverse positions x_o slightly off axis. The electron beam may also have a small energy spread $\Delta\gamma/\gamma$. The energy spread and emittance of the electron beam translate into a spread in phase velocities in phase-space. The phase velocity spread due to energy spread is given by [10]

$$\Delta\nu = 4\pi N \Delta\gamma/\gamma, \qquad (2.49)$$

and the phase velocity spread of an electron beam due to emittance is given by

$$\Delta\nu = -\frac{2\pi N}{1+K^2}\left(K^2 k_o^2 x_o^2 + \gamma^2\theta_x^2\right). \qquad (2.50)$$

Electrons enter the undulator with a spread in phase velocities due to a spread in energies, and are randomly distributed in both the longitudinal and transverse directions. The typical distribution of electron phase velocities is assumed to have a Gaussian form about initial phase velocity ν_o,

$$f_G(q) = \frac{e^{-q^2/2\sigma_G^2}}{\sqrt{2\pi}\,\sigma_G}, \qquad (2.51)$$

where $\sigma_G = 4\pi N \Delta\gamma/\gamma$ is the standard deviation and q is the phase velocity away from ν_o distributed [9]. The characteristic function $F_G(\tau)$ of the distribution $f_G(q)$ is defined as

15

$$F_G(\tau) = \int f_G(q) e^{-iq\tau} dq.$$

Evaluating the above integral equation for a Gaussian yields

$$F_G(\tau) = e^{-\sigma_G^2 \tau^2 / 2}.$$

If the beam quality is perfect so that $\sigma_G = 0$, then $F_G(\tau) = 1$. However, when the beam is not perfect, the characteristic function $|F_G(\tau)|$ decays over the length of the undulator in a characteristic time on the order of $1/\sigma_G$ [9].

Poor beam quality reduces the single-pass FEL gain by degrading electron bunching. As an example, consider an FEL design with $N = 25$ periods having a dimensionless current density of $j = 10$ and initial phase velocity of $v_o = 3$ operating with an initial dimensionless optical field $a_o = 1$. In Figure 2.2, electron beam quality is assumed to be nearly perfect, i.e. $\sigma_G = 1$. Some electrons gain energy and move ahead of the average flow, while other electrons lose energy to the radiation field and move back behind the average flow causing visible spatial bunching.
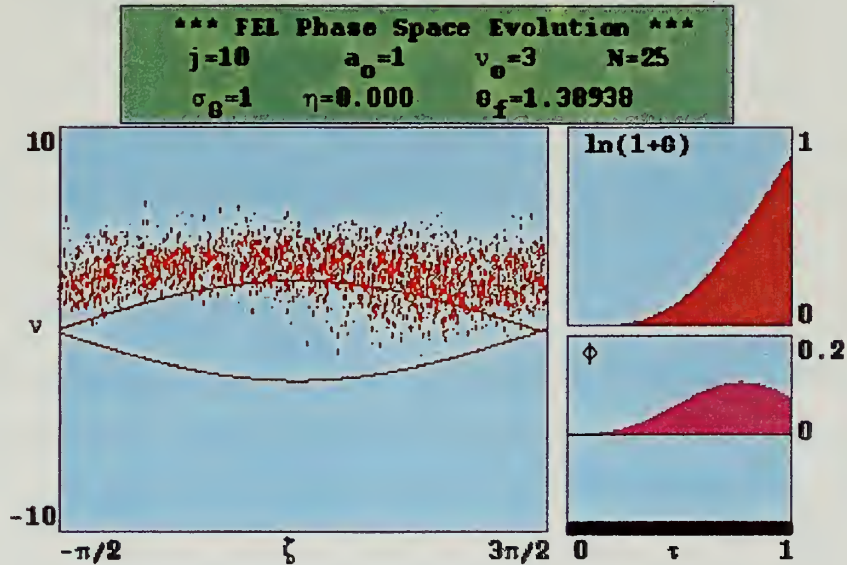

Figure 2.2. Phase space evolution for a nearly perfect electron beam quality.

16

In Figure 2.3, the longitudinal energy spread increases to $\sigma_G = 6$, and this degradation in beam quality causes much less bunching when comparing to Figure 2.2. The poor beam quality is responsible for a decrease in final gain to $G_f = 0.10534$ and a smaller optical phase shift ϕ.
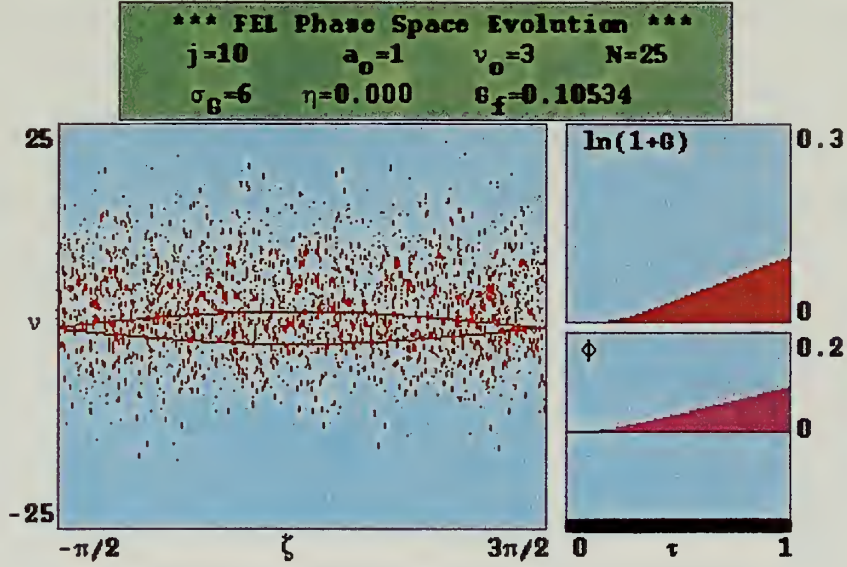

Figure 2.3. Phase space evolution for low gain with electron beam degradation.

F.   TAPERED UNDULATOR

The characteristics of the FEL interaction can be altered by changing the undulator properties, i.e. undulator polarization, wavelength, or field strength, along its length [5]. As an FEL reaches saturation, the electrons have given up enough energy so that they are no longer in resonance with the optical wave, which decreases the gain. Tapering changes the undulator's resonance condition along its length so that the electrons remain in resonance longer, hence increasing the overall gain in strong fields [7]. From the resonance condition (2.12), in order to extract energy out of the electron

17

beam, i.e. reducing γ, and convert into radiation field and still maintain resonance condition, we can either taper the undulator wavelength λ_o, i.e. reducing λ_o, or taper the undulator parameter K, i.e. reducing the undulator field strength B. However, tapering K is easier since the undulator gap needs to be increased to decrease B. Tapering essentially has the same mathematical result as accelerating the electrons. This artificial acceleration is represented by a dimensionless parameter δ. A tapered undulator represents an advantage over the untapered undulator design when the artificial acceleration δ exceeds the deceleration that can be obtained without taper in strong optical fields. When the undulator wavelength is decreased, the artificial acceleration δ is given by $\delta \approx -2\pi N \Delta \lambda_o / \lambda_o$. When the undulator field strength is decreased, $\delta \approx -4\pi N K^2 \Delta B / B(1+K^2)$. With tapering is included in the undulator, the pendulum and wave equations become

$$\overset{\circ\circ}{\zeta} = \overset{\circ}{v} = \delta + |a|\cos(\zeta + \phi), \tag{2.52}$$

$$\text{and } \overset{\circ}{a} = -j < e^{-i\zeta} >,$$

where $\zeta = \int_0^{\tau} k_o(\tau')d\tau' + kz - \omega t$ [10]. The wave equation remains the same, but the simple pendulum equation includes an additional constant torque due to the artificial acceleration δ.

The necessary and desirable criteria for tapering is $|a| > \delta \geq 4|a|^{1/2} \geq 2\pi$. The condition on the left is for trapping electrons in the tapered phase space; the middle condition is that the tapered acceleration exceeds the natural untapered deceleration; and the condition on the right is that the tapered FEL works in the strong field regime [10].

Electrons initially near the phase $\zeta_o \approx 0$ are accelerated by both the strong optical field $|a|$ and the artificial "torque". The electrons initially near $\zeta_o \approx \pi$ undergo a cancellation between the optical field and the torque, leaving them trapped in closed orbits. The taper is effective because electrons near the phase for gain $\zeta \approx \pi$ are trapped, and continue to contribute to the interaction. Electrons near the phase for absorption

$\zeta \approx 0$ are taken away from resonance and eventually stop interacting. The imbalance leads to a net gain [10].

Compared to the untapered undulator, the tapered undulator is more efficient in strong optical fields, but has smaller gain in weak optical fields. The efficiency of a tapered undulator is estimated at $\eta_\delta = \delta/(8\pi N)$. For example, if $\delta \approx 280\pi$ for an undulator with 23% taper in wavelength over $N = 300$ periods, then the efficiency is estimated at $\eta_\delta \approx 70/(2N)$ which increases by a factor of 70 over the natural efficiency $\eta^* \approx 1/(2N)$ [10]. Tapering is a design to obtain higher overall gain and efficiency in strong optical fields.

An example of a tapered undulator in strong optical fields is shown in Figure 2.4 with an untapered undulator shown in Figure 2.5. Both designs are based on an undulator length of $L = 6$ m corresponding to $N = 300$ periods. The dimensionless current density is $j = 12000 \gg \pi$ in the high gain regime, and initial field $a_o = 150 \gg \pi$ in the strong optical field regime. In Figure 2.4, the tapering rate $\delta = 260\pi$ turns on at $\tau_s = 0.19$ along the undulator resulting in a final gain of $G_f = 556$ and FEL extraction efficiency of $\eta \approx 12.5\%$. Initially the gain increases exponentially until $\tau_s = 0.19$ where the taper turns on and saturation is reached. With tapering, the gain continues to increase slowly instead of decreasing after saturation, as shown in the upper right-hand portion of the Figure 2.5. The phase velocity of the untrapped electrons near $\nu \approx 740$ is shifted by the tapering acceleration δ whereas the trapped electrons remain near resonance due to strong optical fields. The lower right-hand portion of the Figure 2.4 is the optical phase shift, and this phase shift $\Delta\phi \approx 1.4\pi$ over the length of the undulator is a characteristic of high gain.
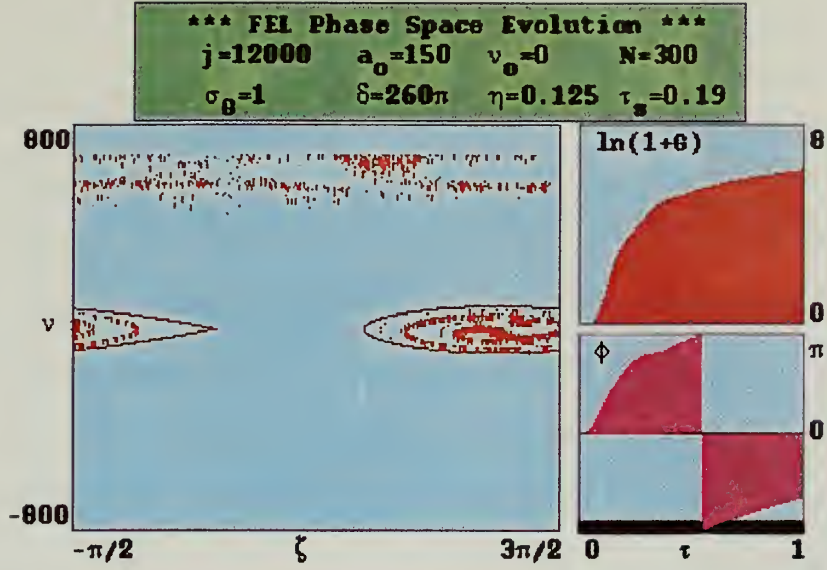
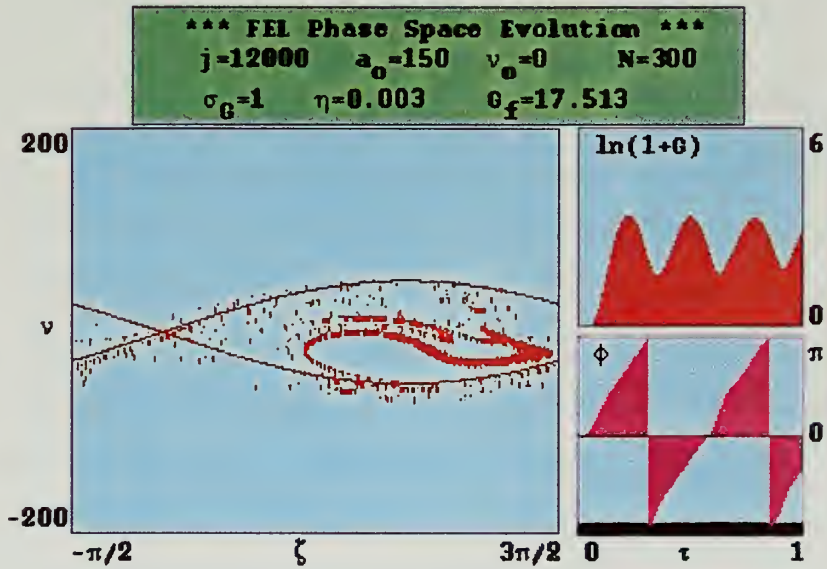Figure 2.4. Phase space evolution for high gain in strong fields with a tapered undulator.

Figure 2.5. Phase space evolution for an untapered undulator.

III. SIMULATIONS OF THE REGENERATIVE
MW FEL AMPLIFIER

A.   MW-CLASS FEL CALCULATIONS

In order to destroy an incoming missile, the laser power required on the missile surface is about 10 kW/cm^2 over a $w_o \approx 5$ cm radius spot for a two second duration. The extinction coefficient due to aerosols at sea level is $\alpha \approx 0.03$ km^{-1}, and through $e^{-\alpha z}$ describes the absorption loss at $\lambda \approx 1\,\mu$m wavelength over a distance z. Let P_t be the Transmitted Power that must leave the ship to destroy a missile at a range R, then the power at the target is $P_d = P_t\, e^{-\alpha R}$. If the range of the missile is 5 km, the laser power which must leave the ship is then $P_t = [10$ kW/cm$^2]\,[\pi(5$ cm$)^2]\,e^{+0.03\text{km}^{-1}5\text{km}} \approx 910$ kW. As an example, consider an FEL with $N = 300$ periods using a beam of 100 MeV electrons with a peak current of 400 A, then the peak electron beam power $\hat{P} = 400$ A$\times 100$ MV ≈ 40 GW. The micropulses generated by the FEL have a length of 0.001 m and are separated by 6 m, then the fraction $D = 0.001/6$ denotes the duty cycle of the FEL. The average power generated within the FEL is given by $\overline{P} = \hat{P} \times D \approx 6.7$ MW. The efficiency necessary to destroy an ASM is $\eta = P_t / \overline{P} \approx 13\%$. Therefore, the single-pass FEL efficiency η needed to supply the Laser Power to destroy the incoming missile is 13%. An approximation of the natural single-pass efficiency of an FEL is only $\eta = 1/2N = 2\%$ so that a tapered undulator with high efficiency is needed. The tapered undulator described in the previous section would be more than adequate. This type of illustration is the essential driving factor in determining the FEL parameters for possible MW-class weapon systems.

B.   LANL REGENERATIVE MW FEL AMPLIFIER

The US Navy is investigating the possibility of using a MW-class Free Electron Laser for ship self-defense against anti-ship missiles (ASM). A design workshop resulted in two possible MW FELs, the oscillator and the regenerative amplifier. The MW oscillator design, although more compact overall, presents a challenge in recirculating an intense electron beam because of a phenomena known as coherent synchrotron radiation (CSR) feedback [11]. The regenerative amplifier design uses a longer undulator and relies on higher extraction efficiency to achieve high average power so that less current is needed from the accelerator and no recirculation is required. The regenerative amplifier design has been proposed by LANL and Boeing with the analysis being performed at NPS. This section explores the analysis of regenerative amplifier design and optimizes its efficiency.

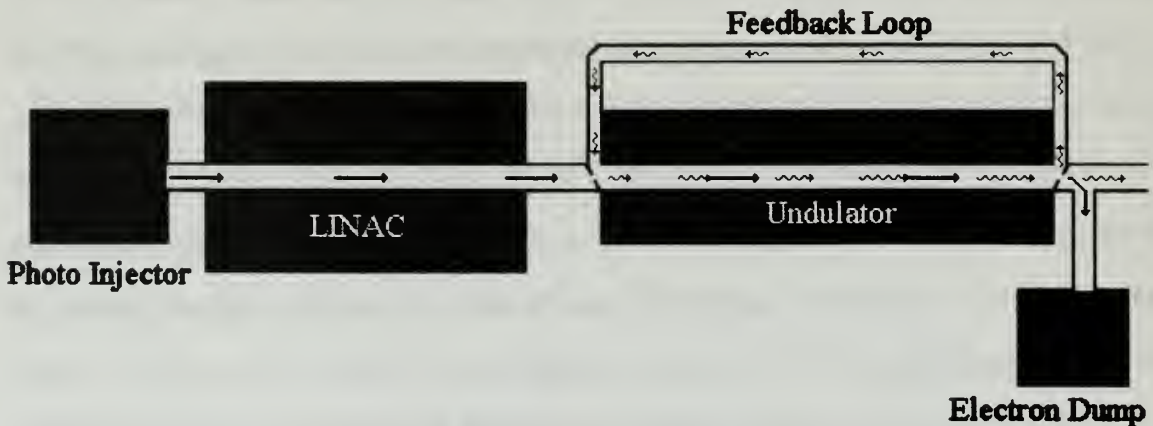A simple schematic of the regenerative amplifier design is shown in Figure 3.1.

Figure 3.1. Conceptual MW class Amplifier FEL.

The amplifier design does not use energy recovery so there is no requirement to bend the high energy beam which can cause deterioration of the electron beam quality. However, without energy recovery, higher extraction efficiency is required. One-dimensional computer simulations are used to describe a single pass of the optical wave and to optimize the efficiency using a tapered undulator. The tapered undulator represents

an advantage when the electron phase acceleration δ exceeds the deceleration that can be obtained without taper in strong optical fields. The single-pass FEL efficiency η of a tapered undulator is the fraction of the electron beam energy converted to laser light. The limit on η is determined by the maximum taper rate δ that can maintain trapped electrons over the number of periods N in the undulator [6]. Gain G is the fractional change in power of the optical field in a single pass through the undulator. In weak fields without tapering, the FEL amplifier has high gain described by $G(\tau) \approx (1/9)e^{\left[(j/2)^{1/3}\sqrt{3}\tau \right]}$ [12]. The gain is exponential in τ along the undulator with growth rate proportional to $j^{1/3}$, where $j = 8N(e\pi KL)^2 \rho F / \gamma^3 mc^2$ is the dimensionless current density, $\rho = 3\times10^9 I(A)/ec\pi r_b^2$ is the electron beam density, and $F =$ "area of electron beam"/"area of light beam" is the filling factor.

Table 3.1 shows the proposed parameters of the MW regenerative amplifier developed at LANL.

Parameters	Proposed Value
Beam energy E	100 MeV
Beam radius r_b	0.17 mm
Energy spread $\Delta\gamma/\gamma$	0.02%
Pulse duration	20 ps
Pulse frequency	500 MHz
Peak current $\hat{I}$	400 A
Average current I	0.2 A
Undulator parameter K	1.71
Undulator length L	6 m
Number of undulator periods N	300
Undulator period λ_o	2.0 cm
Optical wavelength λ	1.0 μm

Table 3.1. Parameters for the MW regenerative amplifier design developed at LANL

1. 1D Efficiency Optimization

The proposed MW RAFEL uses a beam of 100 MeV electrons with a peak current of 400 A, yielding a peak electron beam power of 40 GW. The average current of the RAFEL is 0.2 A, so that the average electron beam power is 20 MW. The single-pass FEL efficiency η is the fraction of power extracted from electron beam in one pass through the undulator. The RAFEL will feedback on the order of 0.01% to 1% of the optical power and require an extraction efficiency of approximately 10% to 15% to provide 2 MW to 3 MW of optical power in the infrared (IR).

In an attempt to achieve the desired efficiency, the initial undulator length is $L = $ 4m corresponding to $N = 200$ periods. The dimensionless initial optical field a_o and tapered undulator of strength δ are varied to find the optimum efficiency. The maximum extraction efficiency found was 8% which is less than the desired efficiency.

In an effort to improve the design efficiency, the length of the undulator is increased from 4 m to 6 m. The change in undulator length corresponds to dimensionless current density of $j \approx 12,000$ with $N = 300$ undulator periods. The values of a_o and δ are varied to find the optimum efficiency using numerical simulations. The electron beam has a Gaussian spread $\sigma_G = 1.0$, and the field strength is $a_o = 150$ with taper rate $\delta = 260\pi$ starting at time $\tau_s = 0.19$ along the undulator. Figure 3.2 is the 3D plot of efficiency versus a_o and δ. The maximum efficiency η_{max} is 13.3% with gain $G = 556$.
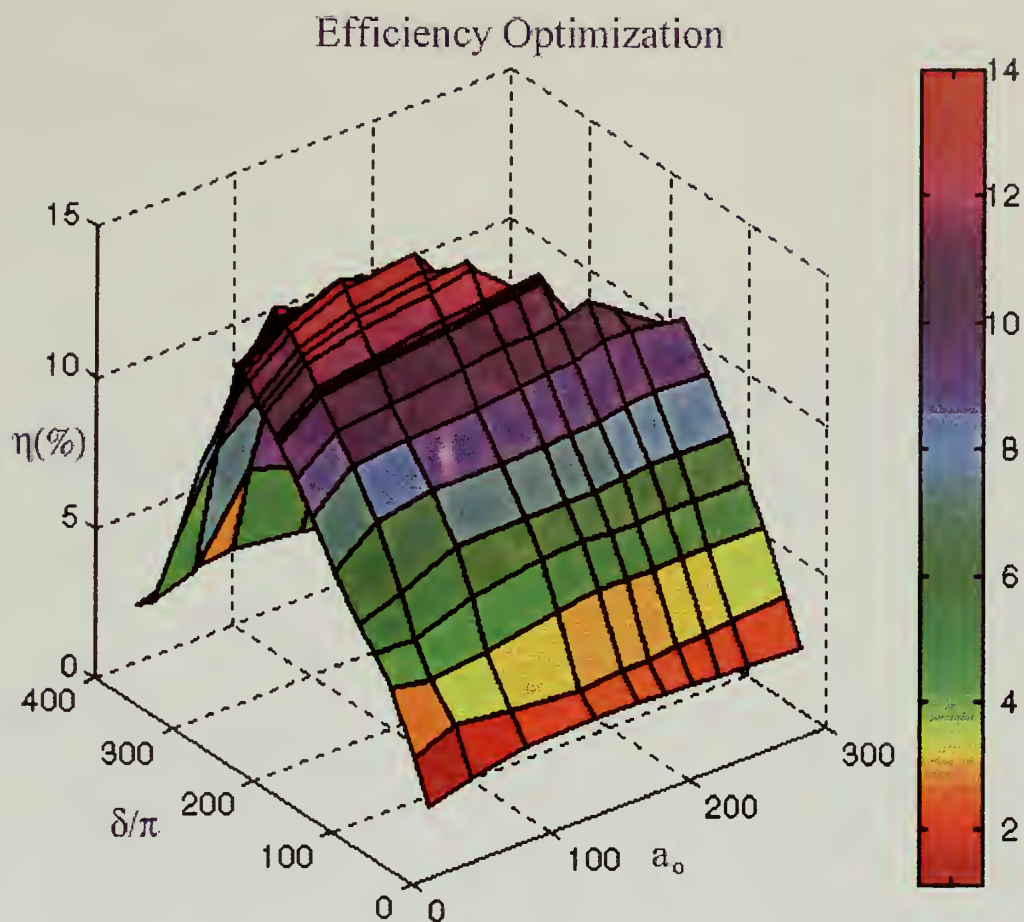
Figure 3.2. 3D plot of Efficiency vs. Optical Field Amplitude
and Tapered Field Strength.

The effect of changing a_o away from its optimum value is smaller than changing δ away from its optimum value as shown in Figure 3.3.
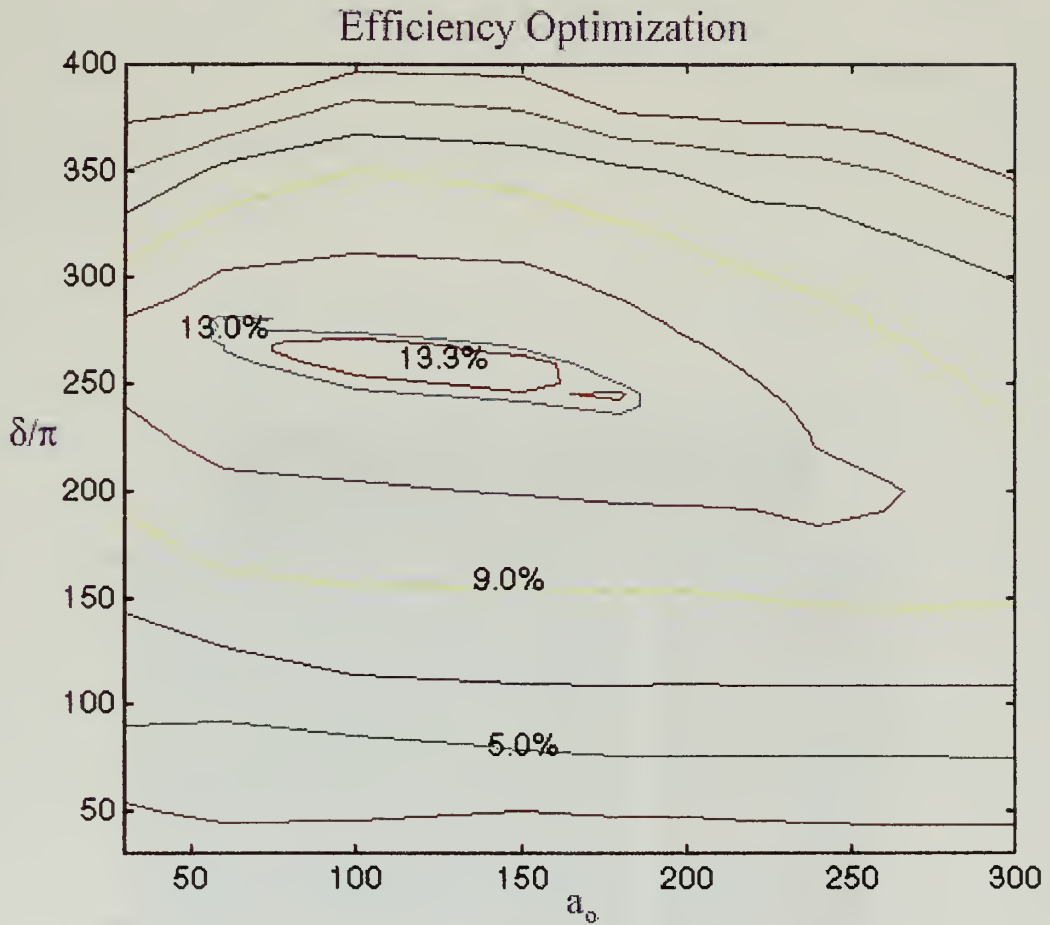

Fig 3.3. Contour plot of Efficiency vs. Optical Field Amplitude and Tapered Field Strength.

For a better understanding of the physical mechanism underlying the operation of this MW RAFEL, examine Figure 3.3 closely in five regions. Region I is the "optimum region". As shown in Figure 3.4, the taper turns on at $\tau_s = 0.19$, and approximately half of electrons were trapped near resonance $\nu_o = 0$, resulting in an acceptable efficiency of $\eta = 13.3\%$. The final gain $G_f = 556$ corresponds to feedback of $f = 1/(G_f + 1) = 1.8 \times 10^{-3}$. The large optical phase shift ϕ in the lower right-hand portion of Figure 3.4 represents good optical guiding which is an important part of a high gain, high current FEL.
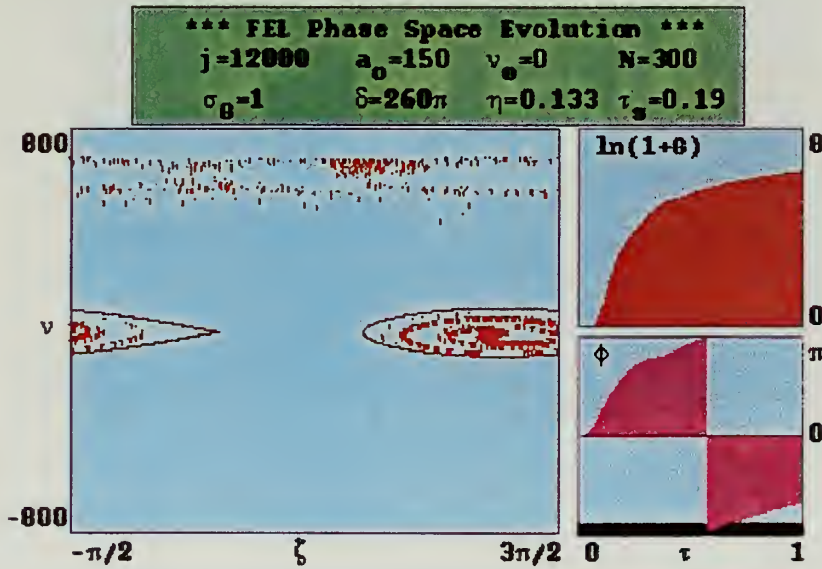
Figure 3.4. Phase space evolution for the MW RAFEL at optimum efficiency.

Region II is the "high tapering rate region". Increasing the tapering rate δ beyond the optimum value, the efficiency drops to 8.3% due to fewer electrons being trapped near resonance $v_o = 0$ as shown in Figure 3.5. The taper turns on at $\tau_s = 0.19$ as before. The final gain $G_f = 347$ corresponds to feedback of $f = 1/(G_f + 1) = 2.9 \times 10^{-3}$. $\overset{\circ}{\phi}$ is relatively small which would cause less optical guiding.
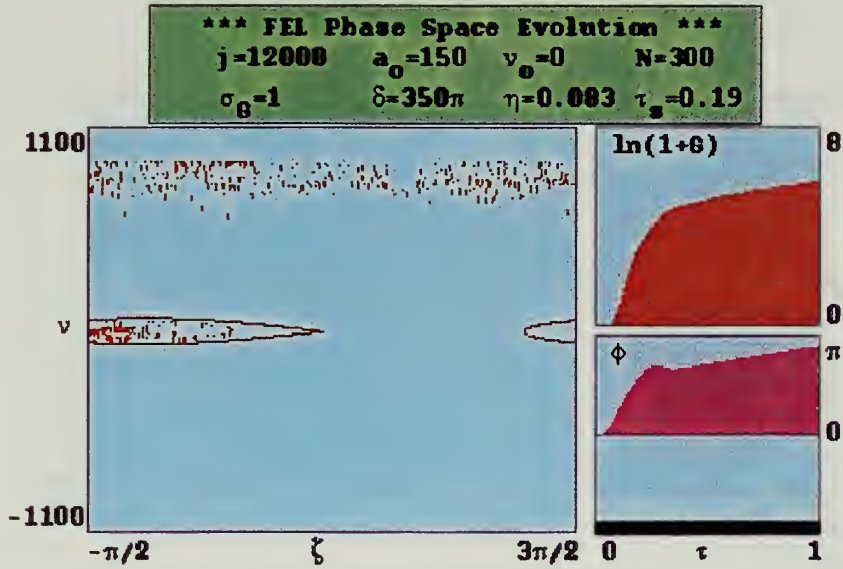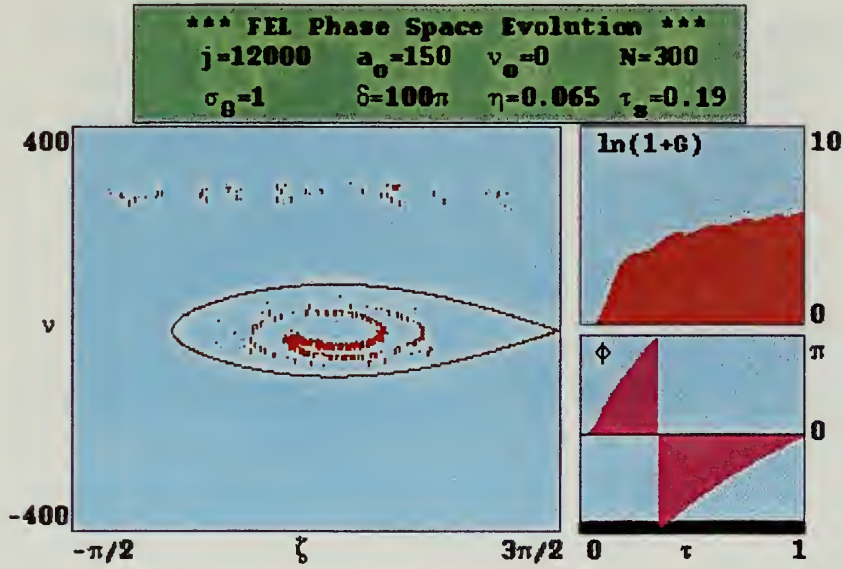

Figure 3.5. Phase space evolution for the MW RAFEL with high tapering rate.

Region III is the "low tapering rate region". For δ below the optimum value, the efficiency drops to 6.5% due to insufficient taper rate as shown in Figure 3.6. While many electrons are trapped near resonance $\nu_o = 0$, the low taper rate does not extract significant energy from them. The taper again turns on at $\tau_s = 0.19$. The final gain $G_f = 294$ corresponding to feedback of $f = 1/(G_f + 1) = 3.4 \times 10^{-3}$.
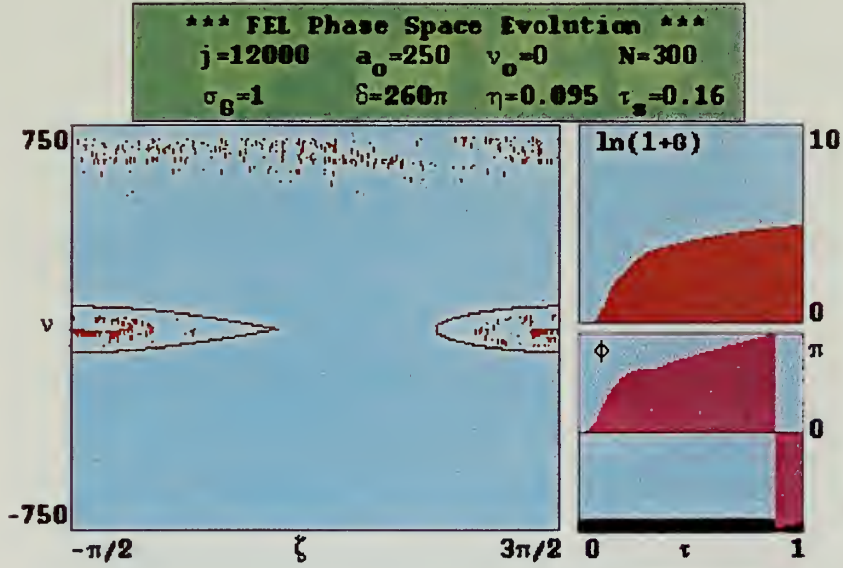

Figure 3.6. Phase space evolution for the MW RAFEL with low tapering rate.

Region IV is the "high optical field region". Starting with high optical field strength a_o, the separatrix does not have a chance to grow and trap electrons, resulting in a lower efficiency of 9.5% as shown in Figure 3.7. The taper turns on at $\tau_s = 0.16$. The final gain $G_f = 144$ corresponds to feedback of $f = 1/(G_f + 1) = 6.9 \times 10^{-3}$.

Figure 3.7. Phase space evolution for the MW RAFEL with high optical field strength.

Region V is the "low optical field region". Starting with low optical field strength a_o, the initial separatrix is too small so that more electrons leak out from the separatrix, resulting in a lower efficiency of 10.9% as shown in Figure 3.8. The taper turns on at $\tau_s = 0.32$. The final gain $G_f = 25,700$ corresponds to feedback of $f = 1/(G_f + 1) = 3.9 \times 10^{-5}$.
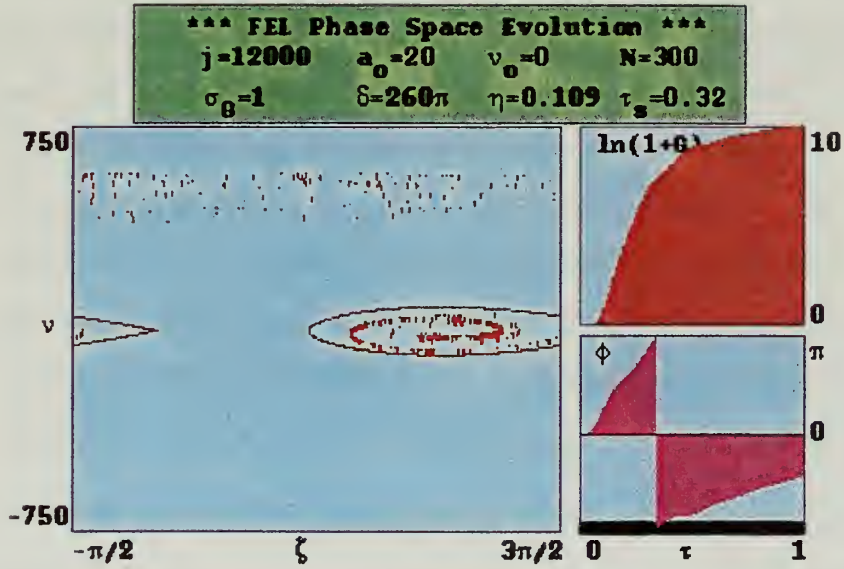

Figure 3.8. Phase space evolution for the MW RAFEL with low optical field strength.

The above results for efficiency should be considered an over-estimate since the effect of diffraction of the optical beam or longitudinal pulse effects are not included.

2. 3D Diffraction Optimization

From Chapter II, the parabolic wave equation can be written as

$$\left[\frac{-i}{4}\nabla_\perp^2 + \frac{\partial}{\partial\tau}\right] a(x,y,z,\tau) = -j\left\langle e^{-i\zeta}\right\rangle. \qquad (3.1)$$

Equation (3.1) governs the dynamics of the optical wave over many optical wavelengths in the longitudinal z-dimension, and the $\nabla_\perp^2$ operator properly describes the diffraction of the optical wave in the transverse (x,y) directions. A coherent, freely-propagating optical wave of radius w_o will spread due to natural diffraction as it traverses the undulator length L. The Rayleigh length, $\pi w_o^2/\lambda$, is the characteristic distance over which the initial optical mode area doubles in size. If the optical mode area becomes much larger than the electron beam, the optical field will decouple from the electron beam. Therefore, it is important that the Rayleigh length is comparable to the undulator length L, and the optical mode waist w_o is not too much larger than the electron beam radius r_b [13].

Three-dimensional simulations are used to describe a single pass of the optical wave through the undulator. Initially, the optimal values from one-dimensional simulation were used as the inputs for a 3D simulation. The resulting 3D simulation is shown in Figure 3.9 with $a_o = 150$, $\delta = 260\pi$, $j = 2.6\times10^4$, and the taper turning on at $\tau_s = 0.2$. The evolution of the optical mode, $|a(x,\tau)|$ shown in the upper-left window of Figure 3.9, is dominated by diffraction after the taper is turned on at $\tau_s = 0.2$. The intense electron beam provides guiding over the first one fifth of the undulator, but after tapering begins diffraction overcomes this focusing over the rest of the undulator. The top-center window shows a cross-sectional view of the optical mode, $|a(x,y)|$, at the end of the undulator, and this optical mode has a drop in optical power in the center. This drop is due to a loss of guiding of the optical mode [14]. The window in the top-right lists the dimensionless parameters for this simulation; σ_x and σ_y correspond to the radial size of the electron beam, while σ_θ and σ_G account for beam quality.

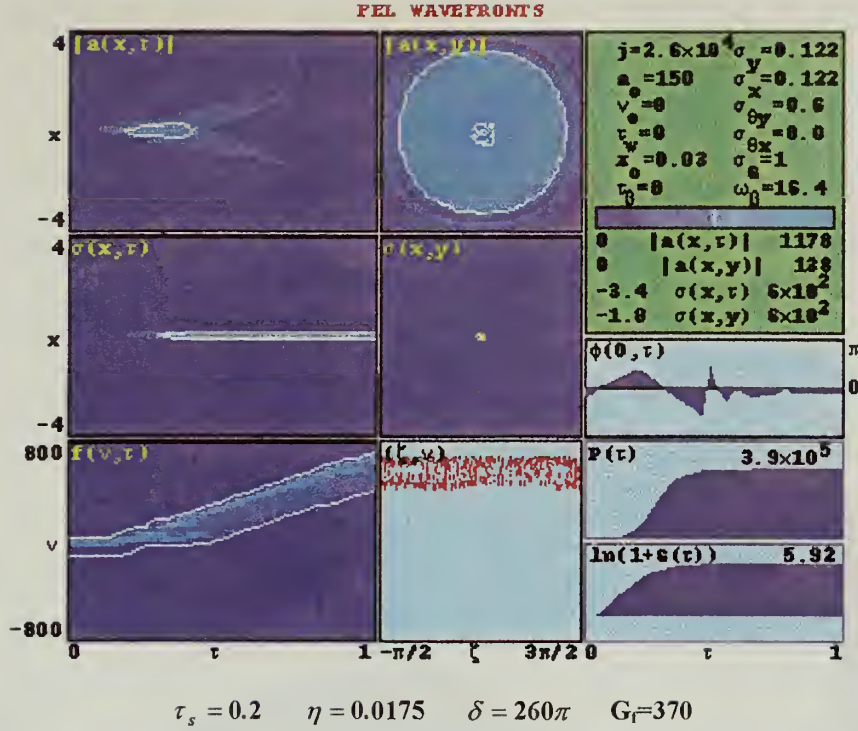$$\tau_s = 0.2 \qquad \eta = 0.0175 \qquad \delta = 260\pi \qquad G_f = 370$$

Figure 3.9. 3D diffraction simulation.

The graph at the right-middle shows the development of the optical phase along the undulator length. At $\tau_s = 0.2$, the optical phase change along the undulator length becomes negative and drops rapidly which causes the optical wavefront to be excluded from the electron beam decreasing the interaction strength. The lower-right window is the plot of the dimensionless optical power growth along the undulator, and the plot of the natural logarithm of the single-pass gain along the undulator. At the middle-left shows the bunching current in the electron beam development along the undulator, with the end view in the center. The bottom-left plot is the electron beam phase velocity evolution along the undulator, and at the bottom center shows the electron phase space plot at the end of the undulator. Initially the optical guiding confines the optical mode until the taper turns on at $\tau_s = 0.2$, then diffraction effects begin to spread the beam. The optical phase begins to grow until the taper turns on, then the change in optical phase is negative as the guiding effect is lost. The bottom-center window shows that at the end of undulator, no electrons are trapped at resonance, and the tapering effect has failed.

33

In order to search for an optimum efficiency using numerical 3D simulations, the initial field a_o, the taper rate δ, and the time to turn on the taper τ_s are varied. The optical field amplitude a_o is varied from 50 to 275 in steps of 25. For each value of a_o, the taper field rate δ is varied from 30π to 330π in steps of 25π, and for each value of a_o and δ, the turn-on time τ_s is varied from 0.1 to 0.5 in steps of 0.02. First we explore the MW RAFEL efficiency by varying δ and τ_s at fixed values of a_o.
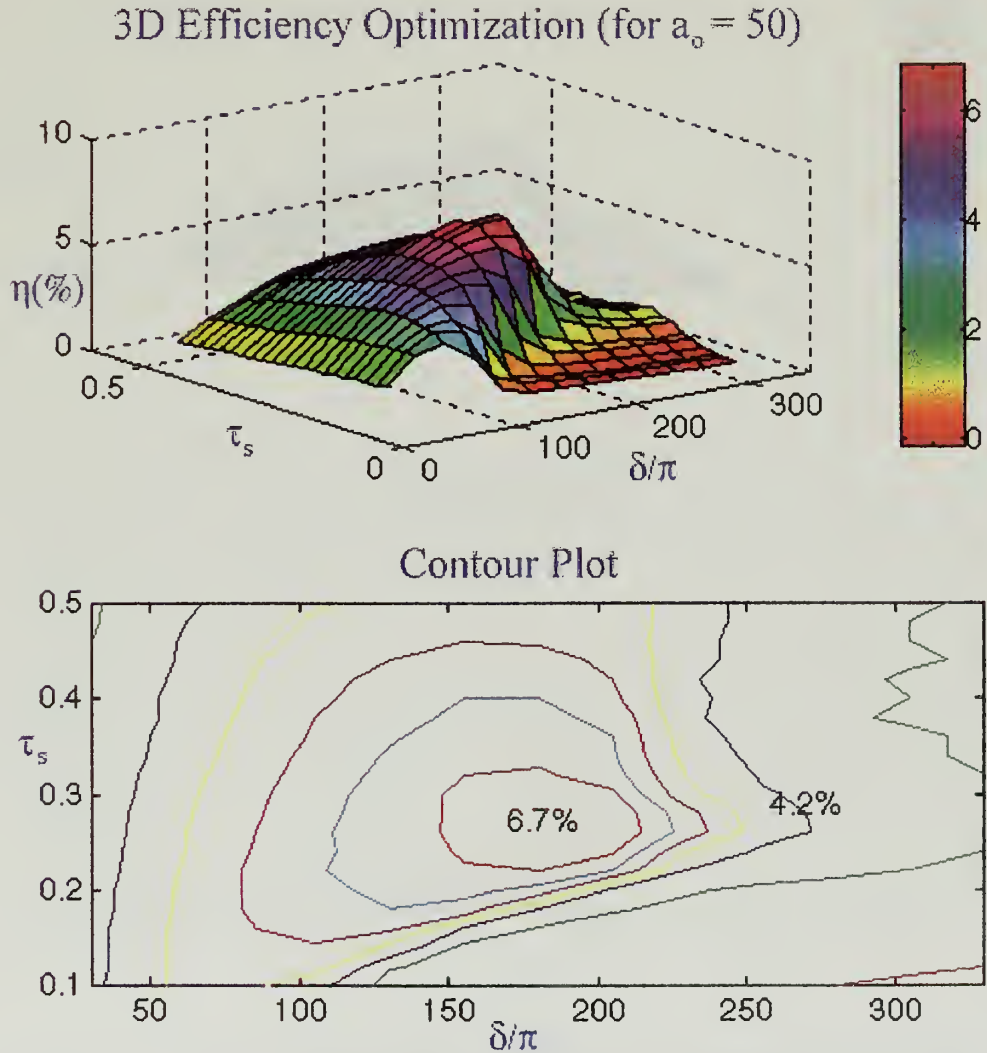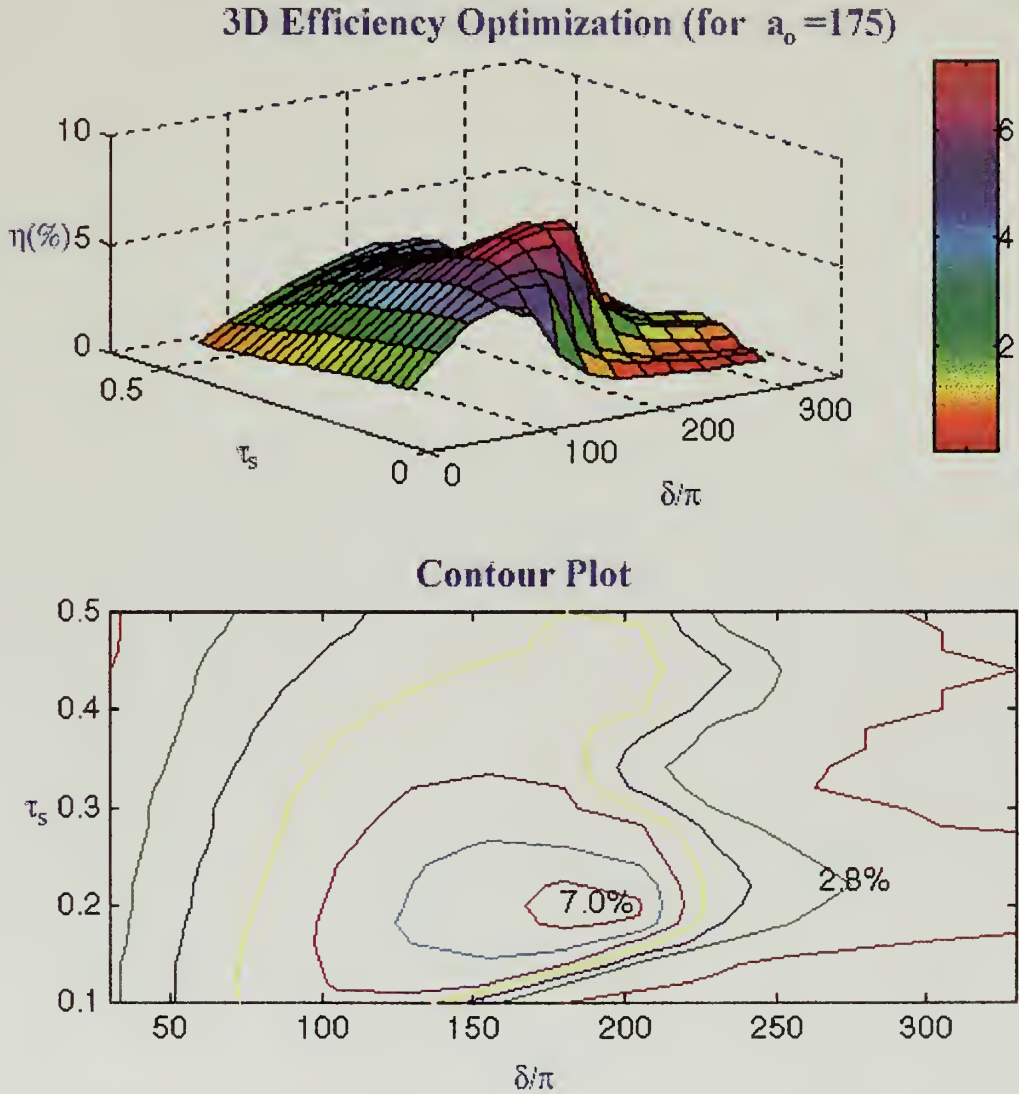

Figure 3.10. 3D and Contour plots of Efficiency vs. Tapered Field Strength and Taper turn-on time at $a_o = 50$.

34

Figures 3.10 through 3.14 show the dependence of efficiency η as τ_s and δ are varied. These two parameters can have a significant impact on efficiency when moved away from their optimum values. The two graphs of each figure are plotted with the same data with the top one is in 3D and the bottom one is in 2D.
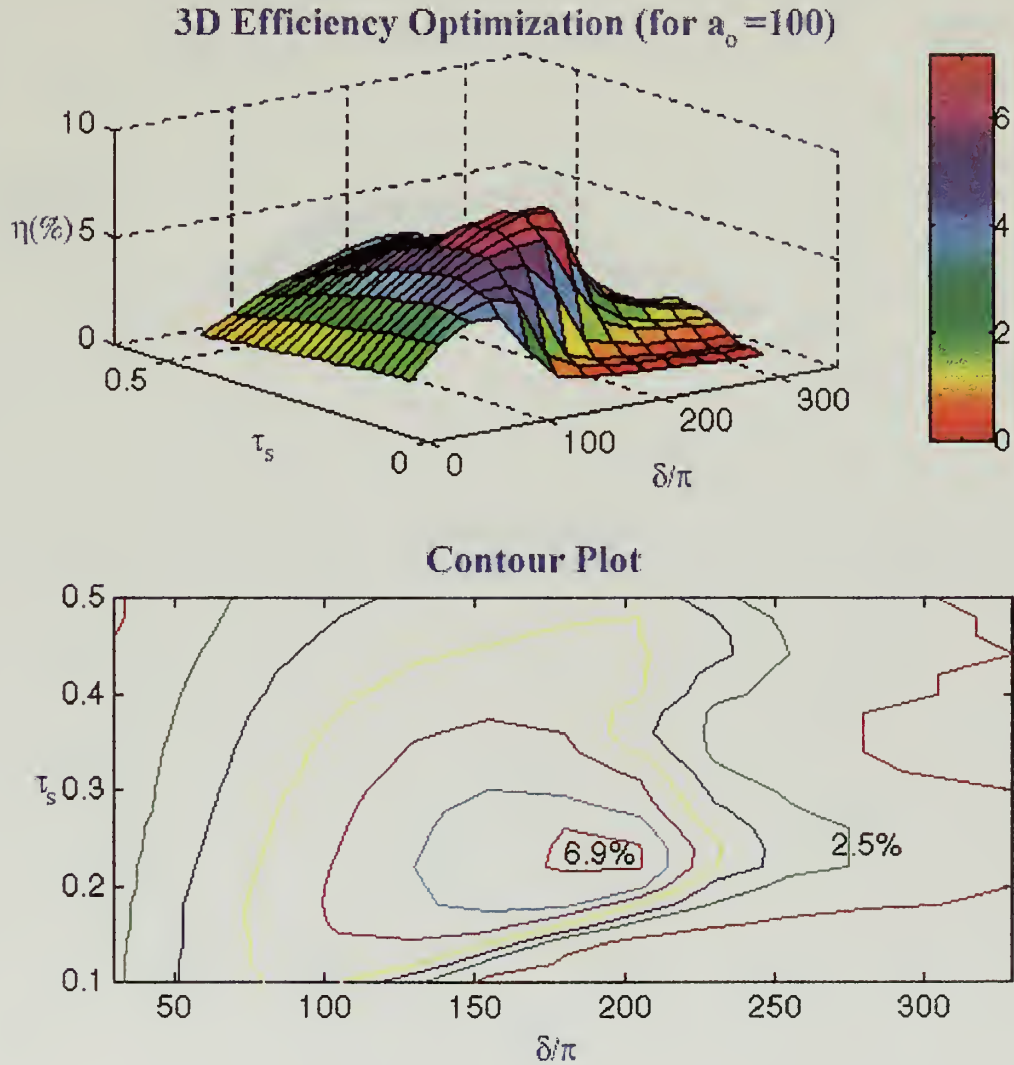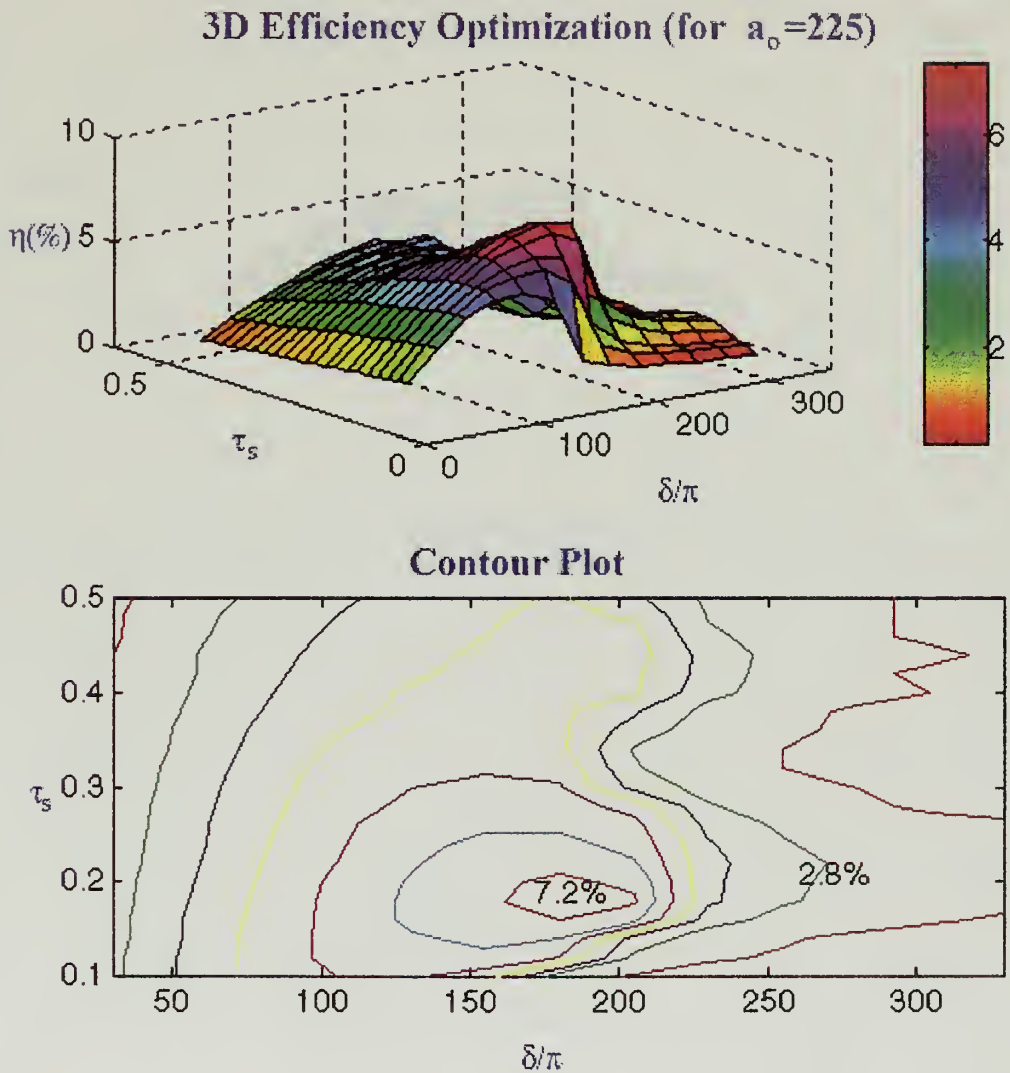

Figure 3.11. 3D and Contour plots of Efficiency vs. Tapered Field Strength and Taper turn-on time at $a_o = 100$.

At the initial optical field amplitude of $a_o = 50$, the efficiency peaks at $\eta_{max} \approx 6.7\%$ at values of $\delta = 200\pi$ and $\tau_s = 0.28$. As a_o increases, the efficiency peaks at slightly higher efficiency $\eta_{max} \approx 7.0\%$ at lower values of $\delta = 190\pi$ and $\tau_s = 0.21$ as shown in Figure 3.12.
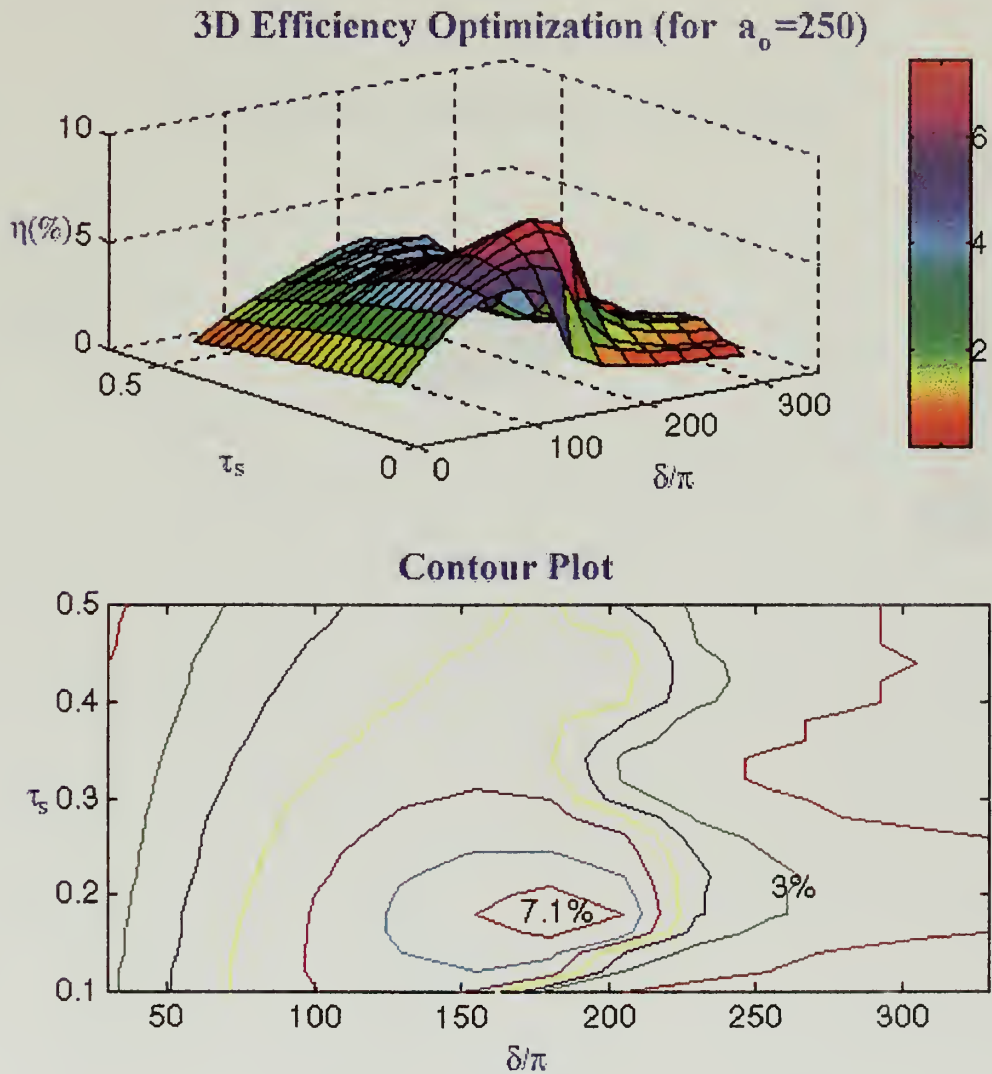

Figure 3.12. 3D and Contour plots of Efficiency vs. Tapered Field Strength and Taper turn-on time at $a_o = 175$.

The peak efficiencies η_{max} continue to increase to a optimum efficiency $\eta_{max} \approx 7.2\%$ corresponding to optimum values $a_o = 225$, $\delta = 180\pi$, and taper turn-on time of $\tau_s = 0.18$ as shown in Figures 3.13.

Figure 3.13. 3D and Contour plots of Efficiency vs. Tapered Field Strength and Taper turn-on time at $a_o = 225$.

Increasing optical field strength a_o beyond its optimum value, the separatrix does not have a chance to grow and trap electrons, resulting in a slightly lower efficiency of 7.1% as shown in Figure 3.14.

Figure 3.14. 3D and Contour plots of Efficiency vs. Tapered Field Strength and Taper turn-on time at $a_o = 250$.

Next, explore the effect on efficiency by varying a_o and τ_s at a fixed value of δ. As shown in Figure 3.15, starting at a low value of the taper field rate $\delta = 55\pi$, the maximum efficiency obtained was 3.2% with $\tau_s \approx 0.2$. This low efficiency is due to insufficient taper rate.

3D Efficiency Optimization (for δ=55π)
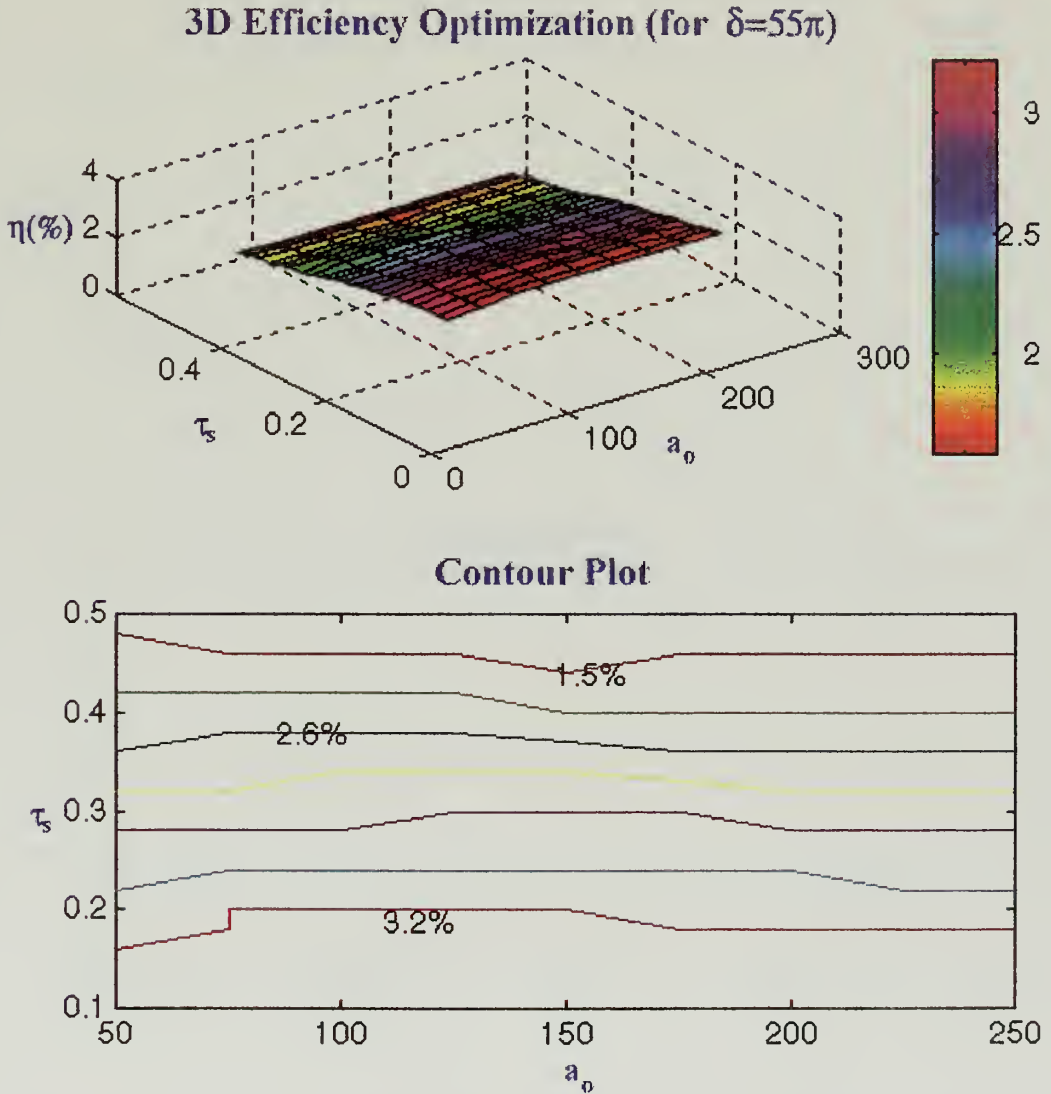
Contour Plot

Figure 3.15. 3D and Contour plots of Efficiency vs. Optical Field Amplitude and Taper turn-on time at $\delta = 55\pi$.

As δ increases, the efficiency increases to $\eta_{max} \approx 5.3\%$ at a slightly lower τ_s as shown in Figure 3.16. The peak efficiency increases to $\eta_{max} \approx 7.2\%$ corresponding to optimum values of $\delta = 180\pi$, a_o =225, and an earlier taper turn-on time of $\tau_s = 0.18$.
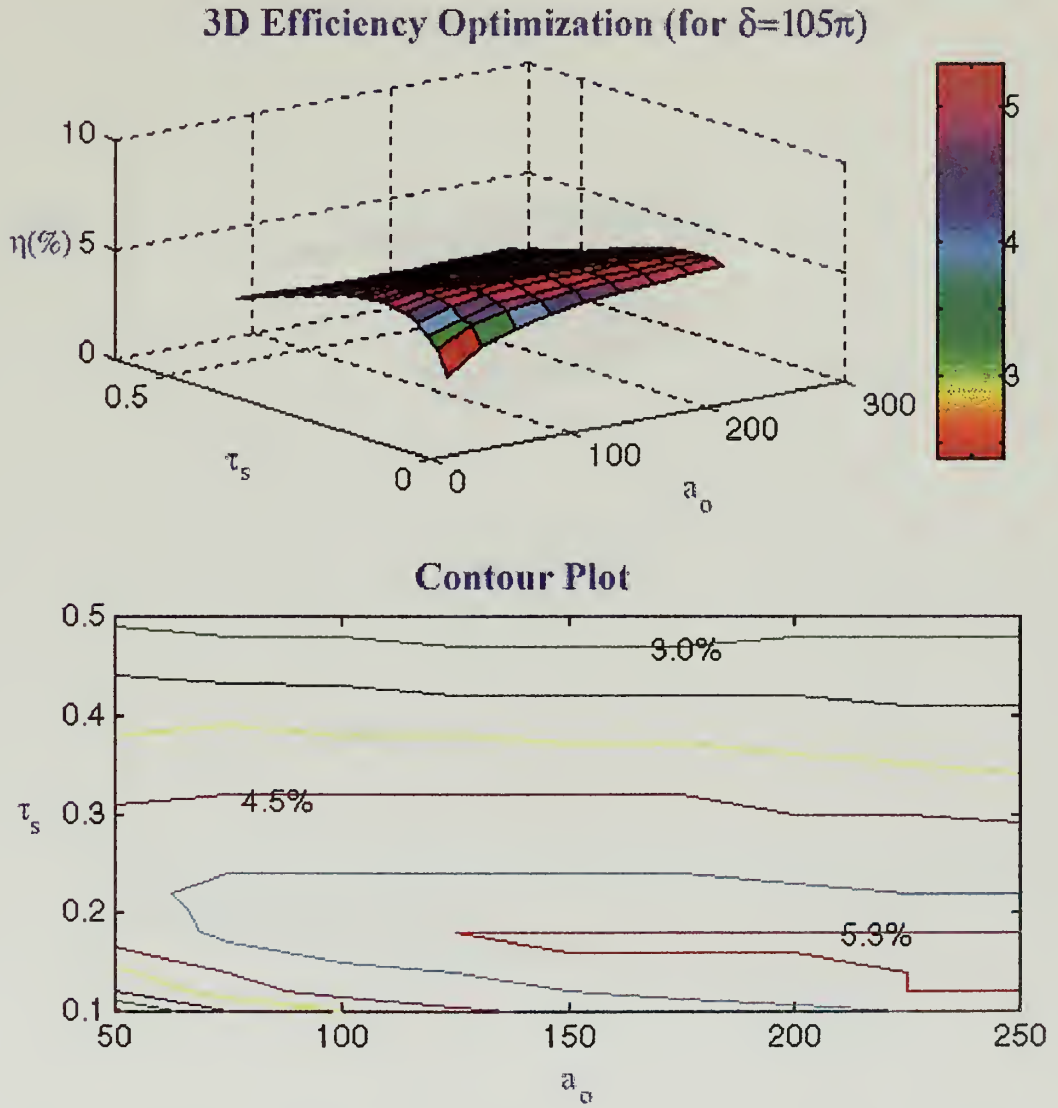

Figure 3.16. 3D and Contour plots of Efficiency vs. Optical Field Amplitude and Taper turn-on time at $\delta = 105\pi$.

As shown in Figure 3.17, when the optimum value of taper rate is used, $\delta = 180\pi$, varying the field a_o has little effect on efficiency, whereas changing the taper turn-on time from its optimum value, $\tau_s \approx 18$, results in a significant efficiency drop.
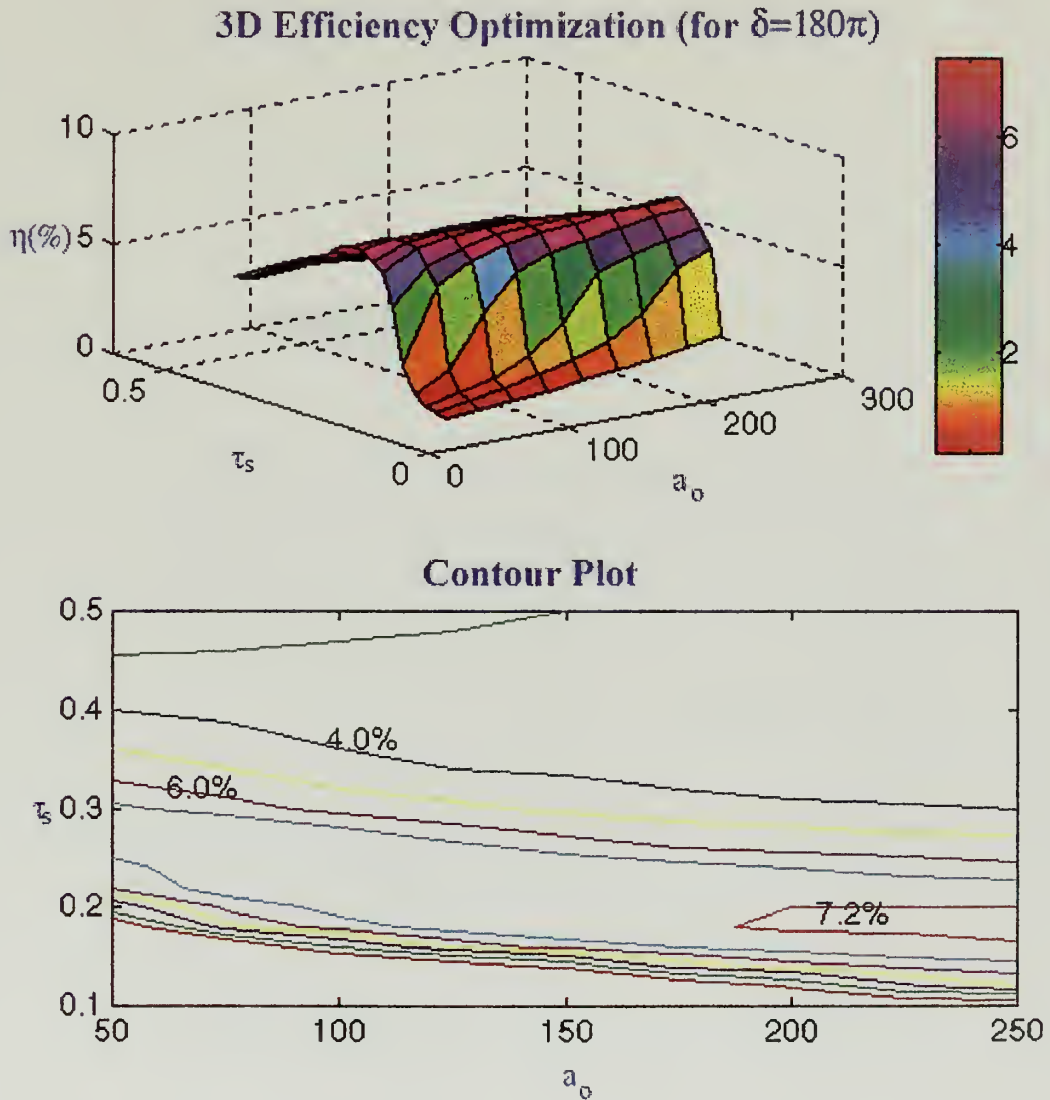

Figure 3.17. 3D and Contour plots of Efficiency vs. Optical Field Amplitude and Taper turn-on time at $\delta = 180\pi$.

Increasing δ beyond its optimum value causes the efficiency to drop significantly due to fewer electron being trapped. As shown in Figure 3.18, the efficiency drops to only 1.9% at $\tau_s = 0.22$ with $\delta = 280\pi$.
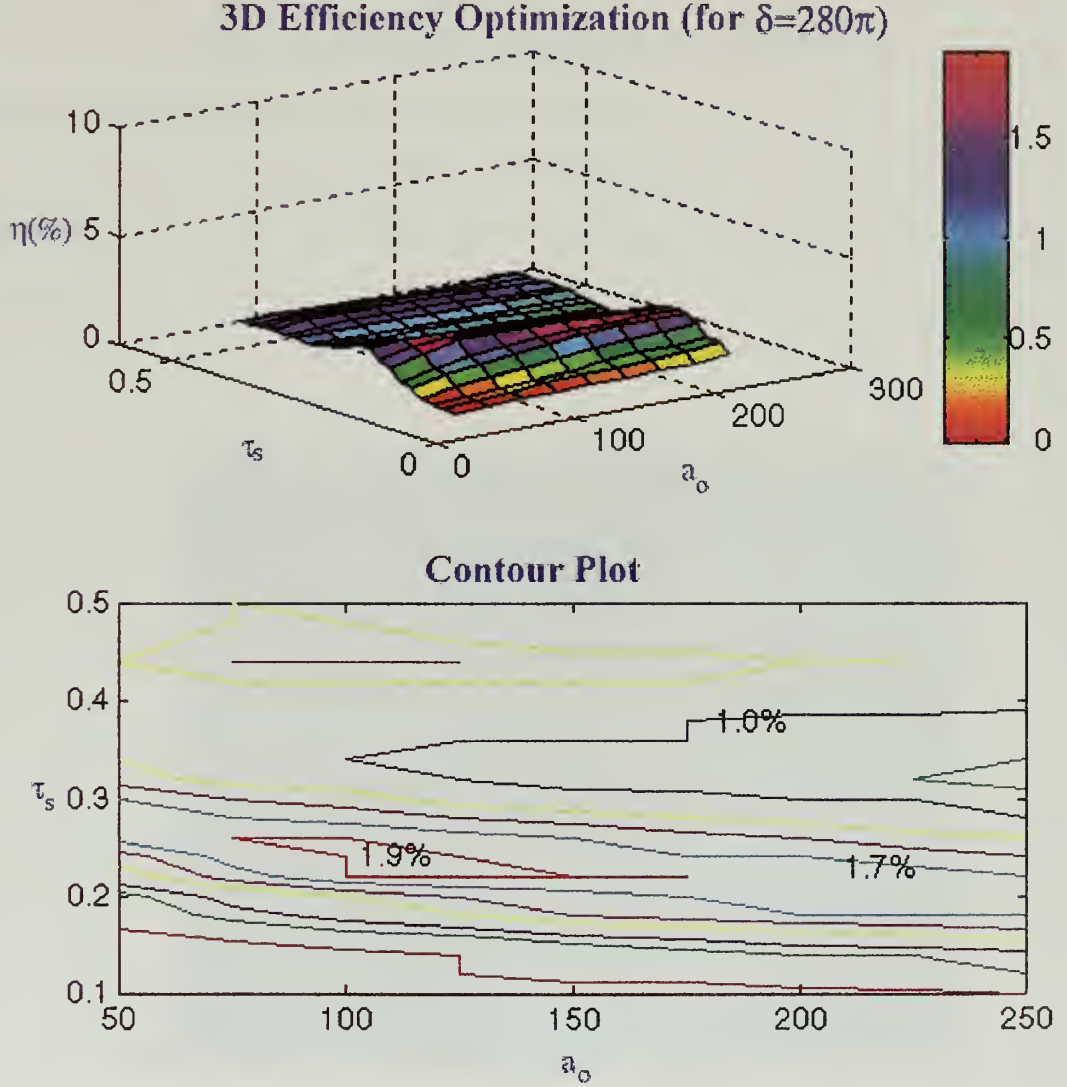

Figure 3.18. 3D and Contour plots of Efficiency vs. Optical Field Amplitude and Taper turn-on time at $\delta = 280\pi$.

Now consider the three-dimensional simulation of a single pass of the optical wave through the undulator at the optimum values of $\delta = 180\pi$, $\tau_s = 0.18$, and $a_o = 225$. As shown in Figure 3.19, optical guiding occurs and stays with the intense electron beam through the undulator as seen in upper-left and middle-left windows. The top-center window shows a much tighter cross-sectional end view of the focused optical power than seen in Figure 3.9. The bottom-center window shows approximately 50% of the electrons are trapped, resulting in optimized gain and efficiency. The middle-right window shows the optical phase initially increasing until the taper turns on at $\tau_s \approx 0.18$, then decreasing slowly. The FEL performance in Figure 3.19 is much improved over that of Figure 3.9. In steady-state operation, the final gain $G_f = 616$ corresponds to feedback of $f = 1/(G_f + 1) = 1.6 \times 10^{-3}$.
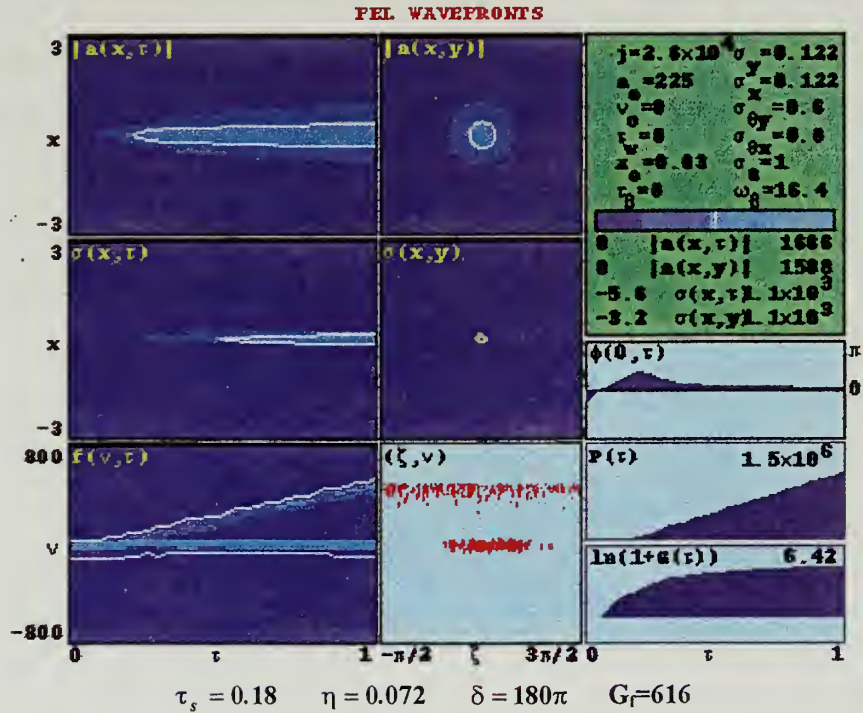

Figure 3.19. 3D diffraction simulation at optimum values
$\delta = 180\pi$, $\tau_s = 0.18$, and $a_o = 225$.

IV.   CONCLUSIONS

The development of a speed-of-light hard-kill weapon system for military applications may represent a significant advancement in technology over present conventional kinetic weapon systems. The FEL has the potential for use as a weapon system against anti-ship and theatre ballistic missiles. The infinite magazine, rapid response, and wavelength tunability at high powers make it suitable and desirable for shipboard self-defense and for land-based theater ballistic missile defense.

Three dimensional computer simulations indicate that the proposed LANL Regenerative MW FEL design does not yield the desired extracted efficiency of $\eta \approx 15\%$. The optical field amplitude a_o, taper rate δ, and taper turn-on time τ_s were varied to search for the optimum efficiency, resulting in maximum efficiency of only $\eta_{max} \approx 7.2\%$. Changing δ or τ_s away from their optimum values has a significant effects on the MW RAFEL design efficiency, but changes in a_o do not have much of an effect. The efficiencies found here are still an over-estimate since they do not include longitudinal pulse effects. It remains to be determined whether a smaller efficiency is acceptable or if 15% efficiency is actually necessary in the FEL weapon design. If 15% efficiency is necessary, a longer undulator, perhaps 8 or 10 meters may be sufficient to reach that goal.

LIST OF REFERENCES

1. J. R. Cook and J R. Albertine, *High Energy Laser Weapon System,* Surface Warfare Magazine, September/October 1997.

2. K. E. Woehler, PH4054 COURSE: *Physics of Directed Energy Weapons*, Naval Postgraduate School, Monterey, CA.

3. C. A. Brau, "*Free Electron Laser*", Academic Press, Inc., San Diego, CA, 1990.

4. W. B. Colson, *Laser Handbook*, Vol. 6, Chapter 1, eds W. B. Colson, C. Pellegrini, and A. Renieri. North-Holland Physics, Elsevier Science Publishing Co. Inc., The Netherlands, 1990.

5. D. Jackson, *Classical Electrodynamics*, 2nd ed., John Wiley & Sons, Inc., 1975.

6. W. B. Colson, Advanced FEL theory Seminar.

7. W. B. Colson, PH4911 COURSE: Simulation of Physical and Weapon Systems, Naval Postgraduate School, Monterey, CA.

8. W. B. Colson, *Laser Handbook*, Vol. 6, Chapter 5, Section 5, eds W. B. Colson, C. Pellegrini, and A. Renieri. North-Holland Physics, Elsevier Science Publishing Co. Inc., The Netherlands, 1990.

9. W. B. Colson, *Laser Handbook*, Vol. 6, Chapter 5, Section 10, eds W. B. Colson, C. Pellegrini, and A. Renieri. North-Holland Physics, Elsevier Science Publishing Co. Inc., The Netherlands, 1990.

10. W. B. Colson, *Laser Handbook*, Vol. 6, Chapter 5, Section 12, eds W. B. Colson, C. Pellegrini, and A. Renieri. North-Holland Physics, Elsevier Science Publishing Co. Inc., The Netherlands, 1990.

11. R. A. Restivo, Master's Thesis, Naval Postgraduate School, 1997.

12. W. B. Colson, *Laser Handbook*, Vol. 6, Chapter 5, Section 8, eds W. B. Colson, C. Pellegrini, and A. Renieri. North-Holland Physics, Elsevier Science Publishing Co. Inc., The Netherlands, 1990.

13.   W. B. Colson, *Laser Handbook*, Vol. 6, Chapter 5, Section 1, eds W. B. Colson, C. Pellegrini, and A. Renieri. North-Holland Physics, Elsevier Science Publishing Co. Inc., The Netherlands, 1990.

14.   E. T. Scharlemann , *Laser Handbook*, Vol. 6, Chapter 9, Section 5, eds W. B. Colson, C. Pellegrini, and A. Renieri. North-Holland Physics, Elsevier Science Publishing Co. Inc., The Netherlands, 1990.

INITIAL DISTRIBUTION LIST